AD-A112 286 UNITED TECHNOLOGIES RESEARCH CENTER EAST HARTFORD CT F/G 12/1
THEORETICAL RESEARCH INVESTIGATION FOR AIR MOLECULAR CALCULATIO--ETC(U)
APR 81 H H MICHELS F19628-80-C-0209

UNCLASSIFIED AFGL-TR-81-0151 NL

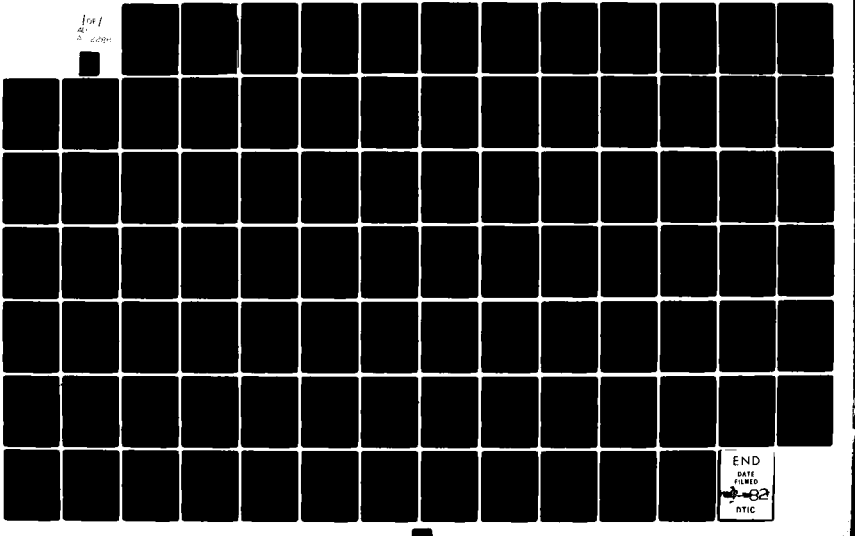

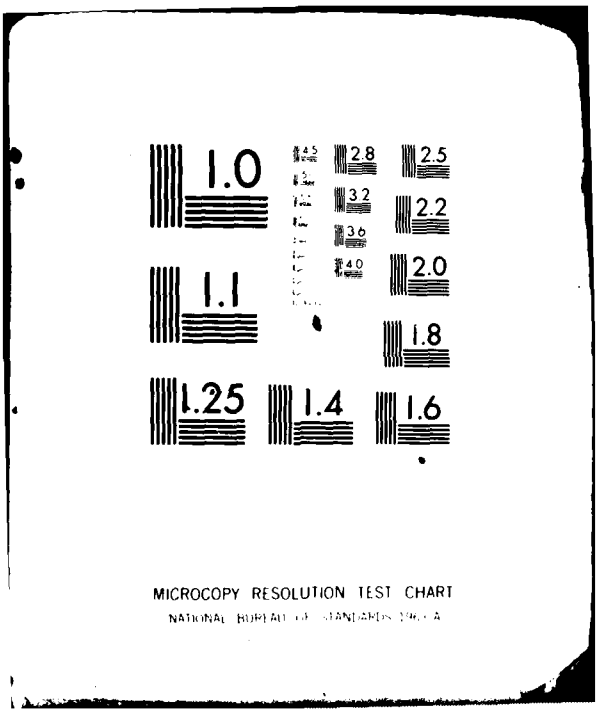
1.0
1.1
1.25
1.4
1.6
1.8
2.0
2.2
2.5
2.8
3.2
3.6
4.0
MICROCOPY RESOLUTION TEST CHART
NATIONAL BUREAU OF STANDARDS 1963-A

AFGL-TR-81-0151

(6)

Theoretical Research Investigation For Air Molecular Calculations

H. Harvey Michels
United Technologies Research Center
East Hartford, Connecticut 06108

15 April 1981
Final Report
80 September 15 - 81 March 15

Approved for public release; distribution unlimited

This research was supported by the Defense Nuclear Agency under Subtask 599QAXHD411, Work Unit 26, Entitled "Reaction Rate Calculations"

Air Force Geophysics Laboratory
Air Force Systems Command
United States Air Force
Hanscom AFB, Massachusetts 01731

Unclassified

SECURITY CLASSIFICATION OF THIS PAGE *(When Data Entered)*

REPORT DOCUMENTATION PAGE	READ INSTRUCTIONS BEFORE COMPLETING FORM
1. REPORT NUMBER: AFGL-TR-81-0151	2. GOVT ACCESSION NO.: AD-A102256
3. RECIPIENT'S CATALOG NUMBER:	
4. TITLE *(and Subtitle)*: THEORETICAL RESEARCH INVESTIGATION FOR AIR MOLECULAR CALCULATIONS	5. TYPE OF REPORT & PERIOD COVERED: Final Report 15 Sept. 1980 - 15 March 1981
	6. PERFORMING ORG. REPORT NUMBER:
7. AUTHOR(s): H. Harvey Michels	8. CONTRACT OR GRANT NUMBER(s): F19628-80-C-0209
9. PERFORMING ORGANIZATION NAME AND ADDRESS: United Technologies Corporation United Technologies Research Center 400 Main Street East Hartford, Connecticut 06108	10. PROGRAM ELEMENT, PROJECT, TASK AREA & WORK UNIT NUMBERS: D411CDAA
11. CONTROLLING OFFICE NAME AND ADDRESS: Air Force Geophysics Laboratory Hanscom AFB, Massachusetts 01731 Monitor/Robert E. Huffman/LKO	12. REPORT DATE: 15 April 1981 13. NUMBER OF PAGES: 92
14. MONITORING AGENCY NAME & ADDRESS*(if different from Controlling Office)*:	15. SECURITY CLASS. *(of this report)*: Unclassified 15a. DECLASSIFICATION/DOWNGRADING SCHEDULE

16. DISTRIBUTION STATEMENT *(of this Report)*

Approved for public release; distribution unlimited

17. DISTRIBUTION STATEMENT *(of the abstract entered in Block 20, if different from Report)*

18. SUPPLEMENTARY NOTES

This research was supported by the Defense Nuclear Agency under Subtask 599QAXHD411, Work Unit 26, Entitled "Reaction Rate Calculations"

19. KEY WORDS *(Continue on reverse side if necessary and identify by block number)*

Ion-Molecule Reaction, Quantum Mechanics, Atomic Oxygen Ion, Nitric Oxide Ion, Aeronomy, N_2O^+

20. ABSTRACT *(Continue on reverse side if necessary and identify by block number)*

The reaction rate of the ion-molecule reaction $O^+ + N_2 \rightarrow NO^+ + N$ has been calculated using quantum mechanical methods. This reaction is important in both the nuclear disturbed and natural ionospheres, since it is a major route for formation of NO^+. The detailed state-to-state cross-sections for this reaction have been calculated as a function of the kinetic energy of the collision and of the vibrational state of nitrogen in its ground electronic state. The energy range used was 0.1 to 10 eV. An examination of the potential energy —

DD FORM 1 JAN 73 1473 EDITION OF 1 NOV 65 IS OBSOLETE (over)

Unclassified

SECURITY CLASSIFICATION OF THIS PAGE *(When Data Entered)*

4A double prime

hypersurfaces involved led to use of the lowest $^4A''$ hypersurface for the reaction. The cross-sections were then calculated using an R-matrix propagator technique. The calculations are in excellent agreement with experiment down to energies of about 0.2 eV, where other mechanisms become dominant. It has been found that increasing either the translational or vibrational energy results in a large increase in cross-section at low energies.

Theoretical Research Investigation
For Air Molecular Calculations

TABLE OF CONTENTS

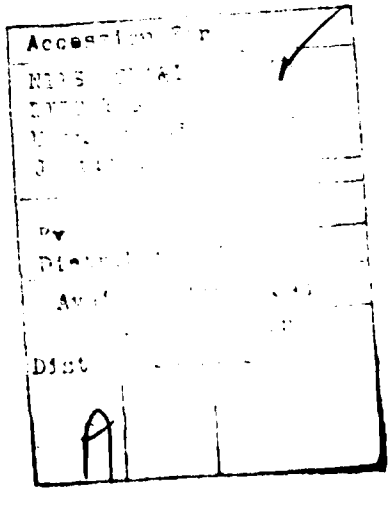

LIST OF ILLUSTRATIONS

LIST OF TABLES

INTRODUCTION

The release of certain chemical species into the upper atmosphere results in luminous clouds that display the resonance electronic-vibrational-rotation spectrum of the released species. Such spectra are seen in rocket releases of chemicals for upper atmospheric studies and upon reentry into the atmosphere of artificial satellites and missiles. Of particular interest in this connection is the observed spectra of certain metallic oxides and air diatomic and triatomic species. From band intensity distribution of the spectra, and knowledge of the f-values for electronic and vibrational transitions, the local conditions of the atmosphere can be determined (Ref. 1).

Present theoretical efforts which are directed toward a more complete and realistic analysis of the transport equations governing atmospheric relaxation, including chemical effects, and the propagation of artificial disturbances require detailed information on atomic and ionic reaction rates and on thermal opacities and LWIR absorption in regions of temperature and pressure where molecular effects are important (Refs. 2 and 3). Although various experimental techniques have been employed for both atomic and molecular systems, theoretical studies have been largely confined to an analysis of the properties (bound-bound, bound-free and free-free) of atomic systems (Refs. 4 and 5). This has been due in large part to the unavailability of reliable wavefunctions for diatomic molecular systems, and particularly for excited states or states of open-shell structures. More recently (Refs. 6-9), reliable theoretical procedures have been prescribed for such systems which have resulted in the development of practical computational programs.

The theoretical analysis of atmospheric reactions requires the knowledge of the electronic structure of atoms, ions and small molecular clusters of nitrogen and oxygen and the interaction of water or other small molecules with these clusters. Knowledge of the chemistry of metal oxide species, which might be present in a contaminated atmosphere, is also desired. In addition the basic collisional processes involving electrons, ions and neutral particles must be understood to evaluate the dynamic effects of the chemistry of the atmosphere. One important reaction is the charge transfer in $N^+ + O \rightarrow N + O^+$. This has been studied experimentally by Neynaber (Ref. 10 and 11) at collision energies between 0.5 eV and 25 eV but low energy (< 0.5 eV) data are apparently extremely difficult to measure.

This reaction has also been investigated theoretically by Michels (Ref. 12) who identified the principle states ($^5\Sigma^+$ and $^5\Pi$) involved in this collision and has carried out charge transfer calculations of the cross-sections for this reaction down to thermal energies.

As an extension of our collisional studies of $N^+ + O$, an examination of the branching ratios in the dissociative-recombination of $e + NO^+ \rightarrow N(^2D, ^4S) + O$ was carried out. The branching into $N(^2D)$ and $N(^4S)$ has been shown by our studies (Ref. 13) to be governed by states of $^2\Sigma^+$ symmetry of NO. Calculations of the branching from an initial recombination into the I $^2\Sigma^+$ state of NO to atomic separations of $N(^4S) + O(^3P)$ and $N(^2D) + O\ (^3P)$ have been carried out. This study utilized the results of our previous research on the electronic structure of NO^+, and NO (Technical Reports AFCRL-TR-75-0509 and AFCRL-TR-76-0120).

Another reaction which is very important in determining the properties of the ionosphere is the ion-molecule reaction:

$$O^+ + N_2 \rightarrow NO^+ + N$$

This reaction provides a major route for the formation of NO^+ and, through dissociative-recombination of $e + NO^+$, the subsequent production of N in the metastable ^2D state. Of particular interest are the detailed state-to-state kinetic cross-sections for this reaction as a function of the kinetic energy of the collision and the vibrational state of N_2 in the ground $X\ ^1\Sigma_g^+$ state. The rates for collisions with metastable $N_2\ A^3\Sigma_u^+$ are also of importance as is the determination of the product distribution which may be vibrationally or electronically excited NO^+, or $N_2^+ + O$ at sufficiently high collision energies.

Because of the difficulty of conducting experiments to measure these unknown cross-sections, the development of a sound theoretical method for calculating these state-to-state processes appears necessary. Although relatively little work of this nature has been done in the past, enough theoretical work is available to indicate that the development of such procedures can be made practical, particularly if good wave functions and potential energy surfaces are available for the interacting species.

The actual calculations of the dynamics of molecular collisions are ordinarily carried out with the aid of the Born-Oppenheimer separation of the electronic and nuclear motion. One proceeds by calculating the electronic energy as a function of the positions of the nuclei, which are assumed to be stationary. This electronic energy, plus the electrostatic repulsion between the nuclei, defines a potential energy hypersurface on which the nuclei may be regarded as moving. A potential energy hypersurface defined in this way is referred to as adiabatic, and is appropriate for describing the nuclear motion in the limit of low velocity. There are many collisions for which an adiabatic potential energy hypersurface provides an adequate description. However, most reactive collisions and many collisions which do not lead to reaction are inadequately described by an adiabatic potential energy hypersurface. These collisions are characterized by velocities of nuclear motion sufficient to affect adversely the Born-Oppenheimer separation, with the result that the overall wavefunction must be described as a superposition of terms involving different electronic energy states. Under these conditions, it will be useful to consider adiabatic potential energy hypersurfaces corresponding to all electronic states relevant to the overall wavefunction.

When the different potential energy hypersurfaces are well separated in energy, the nuclear motion can ordinarily be described in terms of motion on a single hypersurface. However, when two or more hypersurfaces are close in energy, they can be expected to mix appreciably in the overall wavefunction, and it is then necessary not only to calculate the hypersurfaces but also to calculate the quantities needed to discuss their mixing in the overall wavefunction.

The calculation of a point on a potential energy hypersurface is equivalent to calculating the energy of a diatomic or polyatomic system for a specified nuclear configuration, and therefore will present considerable practical computational difficulty. For certain problems or nuclear configurations, the maximum possible accuracy is needed and under these conditions relatively elaborate ab initio methods are indicated. Under other conditions, it may be possible to use less elaborate and more rapid computational methods, and density functional or other approaches may then prove useful.

The research program contained herein was devoted to a theoretical study of the energetics and kinetic reaction rates of $O^+ + N_2$ collisions. The goal of this research program was to develop technical information concerning this system relevant to DNA interests in upper atmospheric reactions.

CURRENT STATUS OF QUANTUM MECHANICAL METHODS FOR DIATOMIC AND POLYATOMIC SYSTEMS

The application of quantum mechanical methods to the prediction of electronic structure has yielded much detailed information about atomic and molecular properties (Ref. 7). Particularly in the past few years, the availability of high-speed computers with large storage capacities has made it possible to examine both atomic and molecular systems using an ab initio approach, wherein no empirical parameters are employed (Ref. 14). Ab initio calculations for diatomic molecules employ a Hamiltonian based on the nonrelativistic electrostatic interaction of the nuclei and electrons, and a wavefunction formed by antisymmetrizing a suitable many-electron function of spatial and spin coordinates. For most applications it is also necessary that the wavefunction represent a particular spin eigenstate and that it have appropriate geometrical symmetry. Nearly all the calculations performed to date are based on the use of one-electron orbitals and are of two types: Hartree-Fock or configuration interaction (Ref. 8).

Hartree-Fock calculations are based on a single assignment of electrons to spatial orbitals, following which the spatial orbitals are optimized, usually subject to certain restrictions. Almost all Hartree-Fock calculations have been subject to the assumption that the diatomic spatial orbitals are all doubly occupied, as nearly as possible, and are all of definite geometrical symmetry. These restrictions define the conventional, or restricted, Hartree-Fock (RHF) method (Refs. 15 and 16). RHF calculations can be made with relatively large Slater-type orbital (STO) basis sets for diatomic molecules with first or second-row atoms, and the results are convergent in the sense that they are insensitive to basis enlargement. The RHF model is adequate to give a qualitatively correct description of the electron interaction in many systems, and in favorable cases can yield equilibrium interatomic separations and force constants. However, the double-occupancy restriction makes the RHF method inappropriate in a number of circumstances of practical interest. In particular, it cannot provide potential curves for molecules dissociating into odd-electron atoms (e.g., NO at large internuclear separation), or into atoms having less electron pairing than the original molecule [e.g., O_2 $^3\Sigma_g^- \rightarrow O(^3P)$]; it cannot handle excited states having unpaired electrons (e.g., the $^3\Sigma$ states of O_2 responsible for the Schumann-Runge bands); and, in general, it gives misleading results for molecules in which the extent of electron correlation changes with internuclear separation.

Configuration-interaction (CI) methods have the capability of avoiding the limitations of the RHF calculations. If configurations not restricted to doubly-occupied orbitals are included, a CI can, in principle, converge to an exact wave-function for the customary Hamiltonian. However, many CI

calculations have in fact been based on a restriction to doubly-occupied orbitals and therefore retain many of the disadvantages of the RHF method (Ref. 8). The use of general CI formulations involves three considerations, all of which have been satisfactorily investigated: the choice of basis orbitals, the choice of configurations (sets of orbital assignments), and the specific calculations needed to make wavefunctions describing pure spin states (Ref. 6). The first consideration is the art associated with quantum mechanical electronic structure calculations. Many methods (iterative NSO, perturbation selection, first order CI, etc.) have been advocated for the optimum choice of configurations. There are not firm rules at present and the optimum choice is a strong function of the insight of the particular research investigator. The last consideration, proper spin and symmetry projection, has proved difficult to implement, but computer programs have been developed for linear projection algebra at this Center, and the CI method has been found of demonstrable value in handling excited states and dissociation processes which cannot be treated with RHF techniques.

Either of the above described methods for ab initio calculations reduces in practice to a series of steps, the most important of which are the evaluation of molecular integrals, the construction of matrix elements of the Hamiltonian, and the optimization of molecular orbitals (RHF) or configuration coefficients (CI). For diatomic molecules, these steps are all comparable in their computing time, so that a point has been reached where there is no longer any one bottleneck determining computation speed. In short, the integral evaluation involves the use of ellipsoidal coordinates and the introduction of the Neumann expansion for the interelectronic repulsion potential (Ref. 17); the matrix element construction depends upon an analysis of the algebra of spin eigenfunctions (Ref. 18), and the orbital or configuration optimization can be carried out by eigenvalue techniques (Refs. 19, 20). All the steps have by now become relatively standard and can be performed efficiently on a computer having 65,000 to 130,000 words of core storage, a cycle time in the microsecond range, and several hundred thousand words of peripheral storage.

Both the RHF and CI methods yield electronic wavefunctions and energies as a function of the internuclear separation, the RHF methods for one state, and the CI method for all states considered. The electronic energies can be regarded as potential curves, from which may be deduced equilibrium internuclear separations, dissociation energies, and constants describing vibrational and rotational motion (including anharmonic and rotation-vibration effects). It is also possible to solve the Schrödinger equation for the motion of the nuclei subject to the potential curves, to obtain vibrational wavefunctions for use in transition probability calculations. The electronic wavefunctions themselves can be used to estimate dipole moments of individual electronic states, transition moments between different electronic states, and other properties. While all of the calculations described in this

paragraph have been carried out on some systems, the unavailability of good electronic wavefunctions and potential curves has limited actual studies of most of these properties to a very small number of molecules.

METHOD OF APPROACH

Central to these studies are the actual quantum-mechanical calculations which must be carried out for the molecular species. For added clarity, various aspects of these calculations are discussed in individual subsections.

1. Levels of Approximation

Much evidence on diatomic and polyatomic systems indicates the near adequacy of a minimum Slater-type-orbital (STO) basis for constructing qualitatively correct molecular wavefunctions (Refs. 21 and 22). This means inner-shell and valence-shell STO's of quantum numbers appropriate to the atoms (1s, 2s, 2p for C, N, O; 1s for H). The main deficiency of the minimum basis set is in its inability to properly describe polarization and the change of orbital shape for systems which exhibit large charge transfer effects. Values of the screening parameters ζ for each orbital can either be set from atomic studies or optimized in the molecule; the latter approach is indicated for studies of higher precision. When high chemical accuracy is required, as for the detailed studies of the ground or a particular excited state of a system, a more extended basis must be used. Double-zeta plus polarization functions or optimized MO's are required for reliable calculated results of chemical accuracy.

The chosen basis sets give good results only when used in a maximally flexible manner. This implies the construction of CI wavefunctions with all kinds of possible orbital occupancies, so that the correlation of electrons into overall states can adjust to an optimum form at each geometrical conformation and for each state. Except when well-defined pairings exist, as for closed shell and exchange dominated systems, a single-configuration study (even of Hartree-Fock quality) will be inadequate.

2. Spin and Symmetry

Proper electronic states for systems composed of light atoms should possess definite eigenvalues of the spin operator S^2 as well as an appropriate geometrical symmetry. The geometrical symmetry can be controlled by the assignment of orbitals to each configuration, but the spin state much be obtained by a constructive or projective technique. Formulas have been developed (Ref. 18) for projective construction of spin states from orthogonal orbitals, and programs implementing these formulas have for several years been in routine use at UTRC.

One of the least widely appreciated aspects of the spin-projection problem is that the same set of occupied spatial orbitals can sometimes be coupled to give more than one overall state of given S quantum number. It is necessary to include in calculations all such spin couplings, as the optimum coupling will continuously change with changes in the molecular conformation. This is especially important in describing degenerate or near-degenerate excited electronic states.

3. Method of Ab Initio Calculation

A spin-free, nonrelativistic, electrostatic Hamiltonian is employed in the Born-Oppenheimer approximation. In systems containing atoms as heavy as N or O this approximation is quite good for low-lying molecular states. For a diatomic molecule containing n electrons, the approximation leads to an electrostatic Hamiltonian depending parametrically on the internuclear separation, R:

$$\mathcal{H}(R) = -\frac{1}{2}\sum_{i=1}^{n}\nabla_i^2 - \sum_{i=1}^{n}\frac{Z_A}{r_{iA}} - \sum_{i=1}^{n}\frac{Z_B}{r_{iB}} + \frac{Z_A Z_B}{R} + \sum_{i>j\geq 1}^{n}\frac{1}{r_{ij}} \qquad (1)$$

where Z_A and Z_B are the charges of nuclei A and B, and r_{iA} is the separation of electron i and nucleus A. $\mathcal{H}$ is in atomic units (energy in Hartrees, length in Bohrs).

Electronic wavefunctions $\psi(R)$ are made to be optimum approximations to solutions, for a given R, of the Schrödinger equation

$$\mathcal{H}(R)\Psi(R) = E(R)\Psi(R) \qquad (2)$$

by invoking the variational principle

$$\delta W(R) = \delta \frac{\int \Psi^*(R)\mathcal{H}(R)\Psi(R)\,d\tau}{\int \Psi^*(R)\Psi(R)\,d\tau} \qquad (3)$$

The integrations in Eq. (3) are over all electronic coordinates and the stationary values of W(R) are approximations to the energies of states described by the corresponding $\psi(R)$. States of a particular symmetry are studied by restricting the electronic wavefunction to be a projection of the appropriate angular momentum and spin operators. Excited electronic states corresponding

to a particular symmetry are handled by construction of configuration-interaction wavefunctions of appropriate size and form.

The specific form for $\psi(R)$ may be written

$$\Psi(R) = \sum_{\mu} c_{\mu} \Psi_{\mu}(R) \tag{4}$$

where each $\psi_{\mu}(R)$ is referred to as a configuration, and has the general structure

$$\Psi_{\mu}(R) = \mathcal{A} \mathcal{O}_S \prod_{i=1}^{n} \phi_{\mu i}(\underset{\sim}{r}_i, R)\, \theta_M \tag{5}$$

where each $\phi_{\mu i}$ is a spatial orbital, $\mathcal{A}$ is the antisymmetrizing operator, $\mathcal{O}_S$ is the spin-projection operator for spin quantum number S, and θ_M is a product of α and β one-electron spin functions of magnetic quantum number M. No requirement is imposed as to the double occupancy of the spatial orbital, so Eqs. (4) and (5) can describe a completely general wavefunction.

In Hartree-Fock calculations $\psi(R)$ is restricted to a single ψ_{μ} which is assumed to consist as nearly as possible of doubly-occupied orbitals. The orbitals $\phi_{\mu i}$ are then selected to be the linear combinations of basis orbitals best satisfying Eq. (3). Writing

$$\phi_{\mu i} = \sum_{\nu} a_{\nu i} \chi_{\nu} \tag{6}$$

the $a_{\nu i}$ are determined by solving the matrix Hartree-Fock equations

$$\sum_{\nu} F_{\lambda \nu} a_{\nu i} = \epsilon_i \sum_{\nu} S_{\lambda \nu} a_{\nu i} \quad \text{(each } \lambda\text{)} \tag{7}$$

where ε_i is the <u>orbital</u> energy of $\phi_{\mu i}$.

The Fock operator $F_{\lambda \nu}$ has been thoroughly discussed in the literature (Ref. 16) and depends upon one- and two-electron molecular integrals and upon the $a_{\nu i}$. This makes Eq. (7) nonlinear and it is therefore solved iteratively. UTRC has developed programs for solving Eq. (7) for both closed and open-shell systems, using basis sets consisting of Slater-type atomic orbitals. Examples of their use are in the literature (Ref. 6).

In configuration interaction calculations, the summation in Eq. (4) has more than one term, and the c_μ are determined by imposing Eq. (3), to obtain the secular equation

$$\sum_\nu (H_{\mu\nu} - w\ _{\mu\nu})\, c_\mu = 0 \qquad (\text{each } \mu) \tag{8}$$

where

$$H_{\mu\nu} = \int \Psi_\mu^*(R)\, \mathcal{H}(R)\, \Psi_\nu(R)\, d\tau$$

$$S_{\mu\nu} = \int \Psi_\mu^*(R)\, \Psi_\nu(R)\, d\tau \tag{9}$$

Equation (8) is solved by matrix diagonalization using either a modified Givens method (Ref. 19) or a method due to Shavitt (Ref. 20).

The matrix elements $H_{\mu\nu}$ and $S_{\mu\nu}$ may be reduced by appropriate operator algebra to the forms

$$H_{\mu\nu} = \sum_P \epsilon_P \left\langle \theta_M \middle| \mathcal{O}_S P \middle| \theta_M \right\rangle \left\langle \prod_{i=1}^{n} \Psi_{\mu i}(\underset{\sim}{r}_i, R) \middle| \mathcal{H}(R) P \middle| \prod_{i=1}^{n} \Psi_{\nu i}(\underset{\sim}{r}_i, R) \right\rangle \tag{10}$$

$$S_{\mu\nu} = \sum_P \epsilon_P \left\langle \theta_M \middle| \mathcal{O}_S P \middle| \theta_M \right\rangle \left\langle \prod_{i=1}^{n} \Psi_{\mu i}(\underset{\sim}{r}_i, R) \middle| P \middle| \prod_{i=1}^{n} \Psi_{\nu i}(\underset{\sim}{r}_i, R) \right\rangle \tag{11}$$

where P is a permutation and ϵ_p its parity. The sum is over all permutations. $\langle\theta_M|\mathcal{O}_S P|\theta_M\rangle$ is a "Sanibel coefficient" and the remaining factors are spatial integrals which can be factored into one- and two-electron integrals. If the $\phi_{\mu i}$ are orthonormal, Eqs. (10) and (11) become more tractable and the $H_{\mu\nu}$ and $S_{\mu\nu}$ may be evaluated by explicit methods given in the literature (Ref. 18). Computer programs have been developed for carrying out this procedure, and they have been used for problems containing up to 64 total electrons, 10 unpaired electrons, and several thousand configurations.

The CI studies described above can be carried out for any orthonormal set of $\phi_{\mu i}$ for which the molecular integrals can be calculated. Programs developed by UTRC make specific provision for the choice of the $\phi_{\mu i}$ as Slater-type atomic orbitals, as symmetry molecular orbitals, as Hartree-Fock orbitals, or as more arbitrary combinations of atomic orbitals.

4. Molecular Integrals

The one- and two-electron integrals needed for the above described method of calculation are evaluated for STO's by methods developed by the present investigators (Ref. 23). All needed computer programs have been developed and fully tested at UTRC.

5. Configuration Selection

Using a minimum basis plus polarization set of one-electron functions, a typical system can have of the order of 10^4 configurations in full CI (that resulting from all possible orbital occupancies). It is therefore essential to identify and use the configurations describing the significant part of the wavefunction. There are several ways to accomplish this objective. First, one may screen atomic-orbital occupancies to eliminate those with excessive formal charge. Alternatively, in a molecular-orbital framework one may eliminate configurations with excessive numbers of anti-bonding orbitals. A third possibility is to carry out an initial screening of configurations, rejecting those whose diagonal energies and interaction matrix elements do not satisfy significance criteria. Programs to sort configurations on all the above criteria are available at UTRC.

Other potentially more elegant methods of configuration choice involve formal approaches based on natural-orbital (Ref. 24) or multiconfiguration SCF (Ref. 25) concepts. To implement the natural-orbital approach, an initial limited-CI wave-function is transformed to natural-orbital form, and the resulting natural orbitals are used to form a new CI. The hoped-for result is a concentration of the bulk of the CI wavefunction into a smaller number of significant terms. The multiconfiguration SCF approach is more cumbersome, but in principle more effective. It yields the optimum orbital choice for a preselected set of configurations. This approach works well when a small number of dominant configurations can be readily identified.

It should be emphasized that the problem of configuration choice is not trivial, and represents an area of detailed study in this research. The existence of this problem causes integral evaluation to be far from a unique limiting factor in the work.

6. Density Function Approach - Xα Model

The Xα model (Ref. 26) for the electronic structure of atoms, molecules, clusters and solids is a local potential model obtained by making a simple approximation to the exchange - correlation energy. If we assume a non-relativistic Hamiltonian with only electrostatic interactions, it can be shown that the total energy E of a system can be written exactly (Ref. 27) (in atomic units) as

$$E = \sum_i n_i \left\langle u_i \left| -\tfrac{1}{2}\nabla_i^2 + \sum_\mu \frac{Z_\mu}{r_{1\mu}} \right| u_i \right\rangle + \tfrac{1}{2} \sum_{\mu \neq \nu} \frac{Z_\mu Z_\nu}{r_{\mu\nu}} \tag{12}$$

$$+ \tfrac{1}{2} \sum_{ij} n_i n_j \left\langle u_i u_j \left| \frac{1}{r_{12}} \right| u_i u_j \right\rangle + E_{xc}$$

This expression is exact provided the u_i are natural orbitals and n_i are their occupation numbers (i.e., eigenfunctions and eigenvalues of the first order density matrix). The first term in Eq. (12) represents the kinetic and electron-nuclear energies. The second term is the nuclear repulsion energy. The sums (μ,ν) are over all the nuclear charges in the system. The third term is the electron-electron repulsion term, which represents the classical electrostatic energy of the charge density ρ interacting with itself, where

$$\rho(1) = \sum_i n_i u_i^*(1)\, u_i(1) \tag{13}$$

The last term E_{xc} represents the exchange correlation energy and can be expressed formally as

$$E_{xc} = \tfrac{1}{2} \int \rho(1)\, d\vec{r}_1 \int \frac{\rho_{xc}(1,2)}{r_{12}}\, d\vec{r}_2 \,, \tag{14}$$

where $\rho_{xc}(1,2)$ represents the exchange-correlation hole around an electron at position 1. In the exact expression, ρ_{xc} is dependent on the second-order density matrix. In the Hartree-Fock approximation E_{xc} is the exchange energy, ρ_{xc} represents the Fermi hole due to the exclusion principle and depends only on the first order density matrix. In the Xα method, we make a simpler assumption about ρ_{xc}. If we assume that the exchange-correlation hole is centered on the electron and is spherically symmetric, it can be shown that the exchange-correlation potential

$$U_{xc} = \int \frac{\rho_{xc}(1,2)}{r_{12}} \, d\vec{r}_2 \tag{15}$$

is inversely proportional to the range of the hole, r_s, where r_s is defined by

$$\frac{4\pi}{3} \, r_s^3 \, \rho(1) = 1 \tag{16}$$

Therefore, in the Xα model, the potential U_{xc} is proportional to $\rho^{1/3}(\vec{r})$. We define a scaling parameter α such that

$$U_{x_\alpha}(1) = - \frac{9\alpha}{2} \, (3\rho(1)/8\pi)^{1/3} \tag{17}$$

The expression in Eq. (17) is defined so that α = 2/3 for the case of a free electron gas in the Hartree-Fock model (Ref. 28) and α = 1 for the potential originally suggested by Slater (Ref. 29). A convenient way to choose this parameter for molecular and solid state applications is to optimize the solutions to the Xα equations in the atomic limit. Schwarz (Ref. 30) has done this for atoms from Z = 1 to Z = 41 and found values between 2/3 and 1.

In the "spin polarized" version of the Xα theory, it is assumed (as in the spin-unrestricted Hartree-Fock model) that electrons interact only with a potential determined by the charge density of the same spin. In this case the contribution to the total energy is summed over the two spins, s = $\pm$ 1/2.

$$E_{xc} = \frac{1}{2} \sum_s \int \rho_s(1) \, U_{x\alpha,s}(1) \, d\vec{r}_1 \tag{18}$$

where the potential is spin-dependent

$$U_{x_{\alpha,s}}(1) = - \frac{9\alpha}{2} \, (3\rho_s(1)/4\pi)^{1/3} \tag{19}$$

and ρ_s is the charge density corresponding the electrons of spin s. The spin-polarized Xα model is useful for describing atoms and molecules with open-shell configurations and crystals which are ferromagnetic or anti-ferromagnetic.

Once one has made the Xα approximation to the total energy functional E in Eq. (12), then the rest of the theory follows from the application of variational principle. The orbitals u_i are determined by demanding that E be stationary with respect to variations in u_i. This leads to the set of one-electron Xα equations

$$\left[-\frac{1}{2}\nabla_1^2 + \sum_{\mu} \frac{z_\mu}{r_{1\mu}} + \int \frac{\rho(2)}{r_{12}} d\vec{r}_2 + \frac{2}{3} U_{x\alpha} \right] u_i = \epsilon_i u_i \qquad (20)$$

where ε_i is the one-electron eigenvalue associated with u_i. Since $\rho(\vec{r})$ is defined in terms of the orbitals u_i, Eq. (20) must be solved iteratively, until self-consistency is achieved. Empirically, if one takes as an initial guess that ρ is approximately a sum of superimposed atomic charge densities, then the convergence of this procedure is fairly rapid. The factor of 2/3 multiplying the potential is a result of the linear dependence of E_{xc} on ρ. This also has a consequence that the Xα eigenvalues ε_i do not satisfy Koopman's theorem, i.e., they cannot be interpreted as ionization energies. However, it can be shown that the ε_i are partial derivatives of the total expression of Eq. (12) with respect to the occupation number,

$$\epsilon_i = \frac{\partial E}{\partial n_i} \qquad (21)$$

If E were a linear function of n_i, then Koopman's theorem would hold. However, because of the dominant Coulomb term, E is better approximated by a quadratic function in n_i. This leads to the "transition state" approximation which allows one to equate the difference in total energy between the state (n_i, n_j) and (n_i-1, n_j+1) to the difference in the one-electron energies $(\varepsilon_j - \varepsilon_i)$ calculated in the state $(n_i - 1/2, n_j + 1/2)$. The error in this approximation is proportional to third-order derivatives of E with respect to n_i and n_j, which are usually small (Ref. 31). The main advantage of using the transition state rather than directly comparing the total energy values is computational convenience, especially if the total energies are large numbers and the difference is small.

The relationship of Eq. (21) also implies the existence of a "Fermi level" for the ground state. This can be seen by varying E with respect to n_i under the condition that the sum $\sum_i n_i$ is a constant, i.e.,

$$\delta\left[E - \lambda \sum_i n_i\right] = 0 \qquad (22)$$

implies $\frac{\partial E}{\partial n_i} = \lambda$, where λ is a Lagrangian multiplier. This implies that the total energy is stationary when all the one-electron energies are equal. However, the occupation numbers are also subject to the restriction $0 \leq n_i \leq 1$. This leads to the following conditions on the ground state occupation numbers;

$$\begin{aligned} (\epsilon_i < \lambda \cdot);\ & n_i = 1 \\ (\epsilon_i > \lambda \cdot);\ & n_i = 0 \\ (\epsilon_i = \lambda \cdot);\ & 0 \leq n_i \leq 1 \end{aligned} \tag{23}$$

In other words, the ground state eigenvalues obey Fermi statistics with λ representing the Fermi energy. It should be noted that, in contrast to the Hartree-Fock theory, where all the n_i are either 0 or 1, the Xα model predicts in some cases, fractional occupation numbers at the Fermi level. In particular, this will occur in a system (such as transition metal or actinide atom) which has more than one open shell.

The Xα model differs in other significant ways from the Hartree-Fock method. In fact, the simplification introduced in approximating the total energy expression introduces several distinct advantages over Hartree-Fock:

1. The primary advantage is purely computational. The one-electron potential in Eq. (20) is orbital-independent and local, i.e., it is the same for all electrons (except in the spin-polarized Xα theory) and is a multiplicative operator. On the other hand, the Hartree-Fock potential is nonlocal, or equivalently, there is a different local potential for each orbital. This involves a great deal more computational effort, especially for systems described by a large number of orbitals. It has been shown (Ref. 32) that the Xα orbitals for the first and second row atoms are at least as accurate as a double-zeta basis set, and are probably better for larger atoms which involve electrons with $\ell \geq 2$.

2. The orbital-independent Xα potential leads to a better one-electron description of electronic excitations of a system. Both the unoccupied ($n_i = 0$) and occupied ($n_i = 1$) eigenfunctions are under the influence of the same potential resulting from the other N-1 electrons. The Hartree-Fock virtual orbitals see a potential characteristic of the N occupied orbitals, and therefore are not as suitable for describing the excited states. Actually although the ground state virtual eigenvalues are usually a good description of the one-electron excitations, the virtual spectrum of the transition state potential where one-half an electron has been removed from the system gives a much better first-order picture of these levels (Ref. 33).

3. As has been shown by Slater (Ref. 34), the Xα model rigorously satisfies both the virial and Hellman-Feynman theorems, independent of the value of the parameter α. This is convenient for calculating the force on a nucleus directly in terms of a three-dimensional integral, rather than the six-dimensional integrals in the expression for the total energy of Eq. (12).

7. Computational Aspects of the Xα Method

In application of the Xα model to finite molecular systems, there are two practical aspects of the calculations which must be considered. The first concerns the choice of the integration framework for describing the molecular wavefunctions and the second deals with the choice of the exchange parameter, α, in different regions of space.

In computations with heteronuclear molecules, there are several free parameters that must be chosen: the ratio of sphere radii for the atomic spheres of integration at a given internuclear separation, the degree of sphere overlap, and the value of the exchange parameter in the atomic spheres and the intersphere region.

It has been found that changing the ratio of the sphere radii for the two atoms in a heteronuclear diatomic molecule introduces changes in the total energy that can be large on a chemical scale ($\sim$ 1 eV). A choice for sphere radii based on covalent bonding radii does not necessarily provide a good estimate for these calculations. The value of the exchange parameter, α, and the sphere radii and/or sphere overlap is normally fixed in Xα calculations for crystals where the geometry is fixed. However, to develop a potential curve, the molecular description needs to change substantially as the internuclear separation varies and the changing sphere radii include varying fractions of the total molecular charge (Ref. 35). Studies made at UTRC have shown that at any given separation the total energy calculated from the Xα model is a minimum at the radii ratio where the spherically averaged potentials from the two atomic centers is equal at the sphere radius.

$$V_1(r_{s_1}) = V_2(r_{s_2}) \tag{24}$$

This relationship between the potential match at the sphere boundary and the minimum in the total energy appears to hold exactly for "neutral" atoms and holds well for ionic molecular constituents. In the case of two ionic species, the long range tail of the potential must go like +2/R from one ion and -2/R (in Rydbergs) for the other ion and so at large internuclear separations, the tails of the potential cannot match well. However, at reasonable separations, the 1/R character of the potential does not invalidate the potential match criterion for radii selection. This match for the atomic potentials is applied to the self-consistent potentials.

In molecules with significant charge sharing in the bonds, the radii of the atomic spheres is frequently increased in Xα calculations so that an overlap region appears in the vicinity of the bond (Ref. 36). Studies made at

UTRC show that the contribution to the total molecular energy from the exchange integral shows a minimum at the optimum sphere radius or sphere overlap. This provides a sensitive criterion for selecting these parameters.

The values of the exchange parameters in the spherical integration region around each atomic center are frequently set at the atomic values both for neutral and for ionic molecular constituents. However, for light atoms, the value of α which best reproduces Hartree-Fock results varies substantially with ionicity. In argon, the following table compares, for the neutral atom and the positive ion, the HF energy and the Xα energy calculated for several values of α.

	α	Xα Energy	HF Energy
Ar^0	.72177	526.8176	526.8173
$Ar^{+1/2}$	.72177	526.5857	-
	.72213	526.6007	-
Ar^{+1}	.72177	526.2447	-
	.72213	526.2596	-
	.72249	526.2745	526.2743

The optimum value of α changes even more rapidly in the fluorine atom, going from 0.73732 for F^0 to 0.72991 for F^{-1}. Since the total energy depends linearly on α, this parameter must be chosen carefully.

The intersphere exchange coefficient is chosen to be a weighted average of the atomic exchange parameters from the two constituents. At small internuclear separations, the optimum radius for an atomic sphere frequently places significant amounts of charge outside that atomic sphere - charge that is still strongly associated with its original center rather than being transferred to the other center or associated with the molecular binding region. To best account for these cases the weighting coefficients are chosen to reflect the origin of the charge in the intersphere (or outersphere region).

$$\alpha_{\text{intersphere}} = \frac{\alpha_{s_1}(Q_{s_1} - Q_1^{o}) + \alpha_{s_2}(Q_{s_2} - Q_2^{o})}{(Q_{s_1} - Q_1^{o}) + (Q_{s_2} - Q_2^{o})} \qquad (25)$$

where $(Q_{s_i} - Q_i^{o})$ is the charge lost from sphere i relative to its atomic value (or ionic value) Q_i^{o} and α_{s_i} is the atomic exchange parameter for sphere i. This value for $\alpha_{\text{intersphere}}$ is calculated dynamically - it is updated after each iteration in the self-consistent calculation.

While for heavy atoms, these changes in the exchange parameter would be small, the α's for small atoms vary rapidly with z (and with ionicity). The correct choice of the exchange parameters influences not only the total energy calculated for the molecule but also in some cases affects the distribution of charge between the atomic spheres and the intersphere region.

8. Charge-Transfer Calculations

Even though low-energy atom-atom reactions play an important role in many physical processes, until recently comparatively little effort has been devoted to acquiring a knowledge of the appropriate cross-sections. In the past, both theoreticians and experimental physicists have found it easier to study high-energy collisions. At these energies, the two colliding particles preserve their identities, and it is possible to treat the interaction between them as a perturbation. There is no guarantee that this procedure, known as the Born approximation, will always converge to the correct result (Ref. 37). As the energy of the colliding particles decreases, it is necessary to take account of the distortion these particles undergo during the collision. The method of perturbed stationary states was developed for calculating charge transfer and electronic excitation cross-sections in relatively slow collisions between heavy particles (Ref. 38). The method has been presented in both wave and impact parameter formalisms. In the first of these, the entire system is treated quantum-mechanically, while in the latter the nuclei are assumed to behave as classical particles, traveling along straight line trajectories, and the time-dependent Schrödinger equation is solved to calculate the probability of various types of electronic transitions (Refs. 39, 40, and 41). Forcing the particles to travel along straight lines limits the validity of the impact parameter method to collisions of several hundred electron-volts or greater (Ref. 42). The wave formulation of the method of perturbed stationary states appears to be one practical method of calculating thermal energy charge-exchange cross-sections. A semi-classical close-coupling method (Ref. 43), based on an average scaling procedure, also offers utility for low to intermediate collision energies.

The use of the wave formalism to study charge-transfer reactions at thermal energies dates back to Massey and Smith's pioneering study of $He^+ + He$ thermal low-energy scattering (Ref. 44). Strictly speaking, their theory is applicable only to resonant charge transfer reactions, $A + A^+ \rightarrow A^+ + A$; however, it can be generalized to study nonresonant charge-transfer reactions as well as charge transfer into excited states. If the origin of coordinates is located at the center of mass of the nuclei of the colliding atoms, the Schrödinger equation for an atomic collision can be written in center of mass coordinates as

$$(H - E) \times (\bar{r}, \bar{R}) = \left(H_o - \frac{\hbar^2}{2M} \nabla_{\bar{R}}^2 - \frac{\hbar^2}{2M} \sum_i \sum_j \nabla_i \cdot \nabla_j - E \right) \times (\bar{r}, \bar{R}) = 0 \qquad (26)$$

where $\bar{r}$ represents the position of the electrons, $\bar{R}$ is the vector joining A to B, H_o is the Hamiltonian for the system when the nuclei are held fixed, M is the reduced mass of the two nuclei, M is the sum of the nuclear masses, and E is the internal energy of the system, including the electronic energy.

Ignoring heavy particle kinetic energy terms in the center of mass system results in a modified form of the adiabatic approximation (Ref. 45) and yields perturbed molecular eigenfunction $\psi_n(\bar{r},\bar{R})$ which satisfy the equation

$$\left(H_0 - \frac{\hbar}{2M}\sum_i\sum_j \nabla_i\cdot\nabla_j\right)\psi_n(\bar{r},\bar{R}) = \epsilon_n(R)\psi_n(\bar{r},\bar{R}) \tag{27}$$

Here $\epsilon_n(R)$ is an electronic energy level of the molecule perturbed somewhat by the appearance of the cross terms. The wave function describing the colliding system, $X(\bar{r},\bar{R})$ can be expanded as

$$X(\bar{r},\bar{R}) = \sum_n \psi_n(\bar{r},\bar{R})F_n(\bar{R}) \tag{28}$$

The various scattering cross sections are determined by the asymptotic behavior of the $F_n(\bar{R})$. These functions are determined by substituting the expansion Eq. (28) into Eq. (26). Making use of the orthogonality of the molecular eigenfunctions, it is easy to derive the following set of coupled differential equations for the $F_n(\bar{R})$

$$\left(-\frac{\hbar^2}{2M}\nabla^2_{\bar{R}} + V_n(\bar{R}) - \frac{\hbar^2 k_n^2}{2M}\right)F_n(\bar{R}) = \sum_m \frac{\hbar^2}{2M}\left\{\langle\psi_n|\nabla^2_{\bar{R}}|\psi_m\rangle F_m(\bar{R}) + 2\langle\psi_n\nabla_{\bar{R}}\psi_m\rangle\cdot\nabla_{\bar{R}}F_m(\bar{R})\right\} \tag{29}$$

where $V_n(R)$ and $\hbar^2k_n^2/2M$ are the potential and kinetic energies of particles in the n^{th} channel. Many of the difficulties associated with trying to calculate thermal energy cross-sections emanate from trying to derive and solve this infinite set of coupled partial differential equations. Until recently, the biggest obstacle in the calculation of low-energy cross-sections has been the inability of theorists to develop accurate molecular eigenfunctions. For those problems for which the molecular eigenfunctions were available, the agreement between theory and experiment has been very reasonable for the amount of computational effort involved. This is true for spin exchange and excitation transfer reactions as well as resonance charge transfer reactions (Refs. 46-50).

Although the molecular wave functions and energies available in the past have not been sufficiently accurate to permit extension of the wave formalism to systems having more than about four electrons, recent advances in calculational techniques, especially for two-center systems, have largely overcome this problem. In particular, recent studies have demonstrated the possibility of producing highly accurate adiabatic electronic wave functions for systems containing as many as 40 electrons (Refs. 6, 17, 51, 52). The availability of these small but flexible wave functions, which have the property of connecting with the correct separated atomic states, increases substantially the chances for successful and practical calculations of cross-sections using the perturbed stationary state technique. This is especially true of charge tranfer into excited states, where a knowledge of a number of the low-lying excited states is required.

Even with a reasonable number of the molecular eigenfunctions, the problem of calculating cross sections is far from solved; this is especially true of charge or excitation transfer into excited states. Many of the existing studies of symmetric resonance reactions are based on the two-state approximation which limits the number of terms in the expansion Eq. (14) to two. Under these conditions, the coupling terms on the right-hand side of Eq. (29) vanish (Ref. 53). We have, then, only to solve two partial differential equations, instead of a system of coupled equations. The situation is not as simple, however, for nonsymmetric reactions or for high-energy collisions involving excitation. For these problems, the coupling terms are the source of the transition and the coupled differential equations have to be solved directly.

While a great deal of effort has gone into deriving formal theories of inelastic and rearrangement collisions, relatively little work has gone into trying to solve the resulting equations. This is especially true of low-energy collisions, where the lack of good molecular wave functions has prevented one from evaluating the terms coupling the different channels. Previous studies which were part of the UTRC research program in the electronic structure of atoms and molecules have been devoted to calculating matrix elements similar to some of the terms coupling the electronic and nuclear motion. Some of the required work involves calculating derivatives of the electronic wave functions with respect to the internuclear distance. This task is made simpler by the use of compact but flexible wave functions such as those studied previously at this center.

The biggest obstacle to calculating low-energy cross sections is the solution of the infinite system or coupled partial differential equations describing the scattering, Eq. (29). The physics of the problem usually serves as a guide to truncating these equations to a system of finite order. A partial wave expansion of the $F_n(R)$ leaves a large number of sets of coupled differential equations (Refs. 54 and 55). Since the number of

equations increases as the collision energy increases, there is no single method for solving these equations. At thermal energies, a direct numerical integration of these equations is feasible (Refs. 56 and 57). At higher energies, when inelastic collisions and charge transfer into excited states becomes important, the trajectories of the incident and scattered particles may be nearly classical (Ref. 58). Under these conditions, it is often possible to use the WKB wave function to obtain approximate solutions to these equations (Ref. 59).

9. R-Matrix Propagator Solution for Charge Transfer Reactions

The theory of heavy particle charge transfer is complicated by the fact that, in general, no simple natural coordinate system exists for which a uniform description of reactant and product states can be written. Considering the reaction:

$$O^+[^4S] + N_2[X\,^1\Sigma_g^+] \rightarrow NO^+[X\,^1\Sigma^+] + N[^4S] \tag{30}$$

The internal coordinates describing N_2 cannot be uniformly mass-scaled to represent NO^+ formed as product. A natural coordinate system for such a collision has been described by Marcus (Ref. 60), but this yields very complicated forms for the kinetic energy operator and presents enormous computational difficulties.

Recently, Stechel, et al. (Ref. 61) have described an approach in which two separate nonorthogonal frameworks are employed to describe reactant and product states. The total scattering wavefunction is written as:

$$\psi = \psi^{\alpha}(R,\rho_{\alpha}) + \psi^{\gamma}(R,\rho_{\gamma}) \tag{31}$$

where α and γ represent reactant and product states, respectively. Expanding each as a linear combination of wavefunctions of the type:

$$\psi^i = \sum_j f_j^i(R)\,\phi_j^i(\rho_i) \tag{32}$$

they show that a unique connection between reactant and product states can be achieved, provided the basis functions, $\{\phi^i(\rho_i)\}$ are taken to be nonorthogonal, i.e., $S^{\alpha\gamma} = \langle\phi^{\alpha}|\phi^{\gamma}\rangle \neq 0$.

We note that Eq. (32), in molecular language, is a product wavefunction of the valence-bond type. We also note that an SCF or MCSCF framework for Eq. (32) is not appropriate for treating the collisional aspects of $O^+ + N_2$ due to the orthogonality constraints that must be imposed on such wavefunctions. The use of nonorthogonal basis functions is simplified through the application of

projection algebra techniques for the construction of wavefunctions of overall symmetry. Efficient computer codes for implementing such techniques has been developed in this Research Center over the past years and can be utilized in constructing the proper asymptotic reactant and product state channels.

The solution of the charge exchange problem can be accomplished using a direct Numerov integration of the Schrödinger equations arising from the basis representation of Eq. (32). Alternatively, the R-matrix propagator method, originally formulated by Diestler (Ref. 62), can be employed. This approach relates the known asymptotic solution in the reactant channel to that in the product channel through a series of recursive steps. Defining the normal derivative to the surface R = constant by $\nabla_n \Psi(R,\rho)$, we seek a propagator operator of the form:

$$\psi(R,\rho) = \underset{\sim}{R}_i \nabla_n \psi(R,\rho) \tag{33}$$

The explicit matrix representation of this operator can be written as:

$$\psi\left[R_i - \frac{h_i}{2}, \rho\right] = -\underset{\sim}{r}^i_1 \nabla_n \psi\left[R_i - \frac{h_i}{2}, \rho\right] + \underset{\sim}{r}^i_2 \nabla_n \psi\left[R_i + \frac{h_i}{2}, \rho\right] \tag{34}$$

$$\psi\left[R_i + \frac{h_i}{2}, \rho\right] = -\underset{\sim}{r}^i_3 \nabla_n \psi\left[R_i - \frac{h_i}{2}, \rho\right] + \underset{\sim}{r}^i_4 \nabla_n \psi\left[R_i + \frac{h_i}{2}, \rho\right] \tag{35}$$

Stechel, et al. (Ref. 61), have given explicit expressions for constructing the components of this operator, both in the asymptotic and overlap regions of the interaction. The initial boundary condition in the reactant channel is $\underset{\sim}{R}^i = 1/\lambda_i$, where λ_i is the eigenvalue of the reactant target (in this case, N_2). The accuracy in developing the final R-matrix depends on the chosen step size, h_i, which is taken as an adjustable parameter that can be optimized during the course of the propagator solution.

We have recently implemented this R-propagator analysis at UTRC, using a modified version of the code developed by Stechel, et al. (Ref. 61). One application has been the low-energy collisional de-excitation reaction:

$$N^*[^2D] + O[^3P] \rightarrow N[^4S] + O[^3P] \tag{36}$$

which occurs along a curve-crossing $^2\Sigma^+ - {}^2\Sigma^+$ potential surface. The results of this study have been reported in AFGL-TR-79-0190 (Ref. 12) and are presently being prepared for journal publication.

10. Spin-Projected Unrestricted Hartree-Fock Method

The unrestricted Hartree-Fock (UHF) method developed by Pople and Nesbet (Refs. 63 and 64) yields the best single-determinant approximation to the exact wavefunction for an atomic or molecular system. Such a wavefunction incorporates correlation by allowing orbitals of different spin to adjust to spatially different forms, thus breaking the symmetry restrictions of the conventional (RHF) method (Refs. 15 and 16). It is necessary, however, to project from such a wavefunction, a properly antisymmetrized spin and angular momentum state in order to define eigenstates and eigenenergies corresponding to observable spectroscopic states.

Let $|\alpha>$, $|\beta>$ refer to the doubly-occupied molecular orbitals (MO's), ϕ_α, ϕ_β. Let $|\gamma>$, $|\delta>$, $|\tau>$ refer to the singly occupied MO's. We assume that all MO's have been subjected to a transformation to orthogonal form. Let $C_{\gamma\delta}$ be the coefficient associated with the permutation $\gamma \leftrightarrow \delta$ (this permutation is (-1) times the overlap of the permuted spin eigenfunction with the original spin eigenfunction), and adopt the convection $C_{\gamma\gamma} = -1$. Then the expectation value of the nonrelativistic Hamiltonian

$$\mathcal{H} = \sum_i U(i) + \sum_{i<j} V(i,j) \tag{37}$$

is given by

$$\begin{aligned} <\mathcal{H}> = {} & 2\sum_\alpha <\alpha|U|\alpha> + \sum_\gamma <\gamma|U|\gamma> + 2\sum_{\alpha\beta} <\alpha\beta|V|\alpha\beta> \\ & - \sum_{\alpha\beta} <\alpha\beta|V|\beta\alpha> + 2\sum_{\alpha\gamma} <\alpha\gamma|V|\alpha\gamma> - \sum_{\alpha\gamma} <\alpha\gamma|V|\gamma\alpha> \\ & + \tfrac{1}{2}\sum_{\gamma\delta} <\gamma\delta|V|\gamma\delta> + \tfrac{1}{2}\sum_{\gamma\delta} C_{\gamma\delta} <\gamma\delta|V|\delta\gamma> \end{aligned} \tag{38}$$

where i, j refer to electron numbers, α, β.. γ, δ etc., refer to MO's and the sums run over all α, β....

The equations for determining the optimum MO's can be derived from the following variational form

$$\delta\left[\langle\mathcal{H}\rangle - 2\sum_{\alpha\beta}\epsilon_{\alpha\beta}\langle\alpha|\beta\rangle - \sum_{\alpha\beta}\left(\epsilon_{\gamma\alpha}\langle\alpha|\gamma\rangle + \epsilon_{\alpha\gamma}\langle\gamma|\alpha\rangle\right) - \sum_{\gamma\delta}\epsilon_{\gamma\delta}\langle\gamma|\delta\rangle\right] = 0 \quad (39)$$

These equations are

$$\left(U + 2J_c - K_c + J_o - \tfrac{1}{2}K_o\right)|\alpha\rangle = \sum_{\beta}\epsilon_{\beta\alpha}|\beta\rangle + \tfrac{1}{2}\sum_{\delta}\epsilon_{\delta\alpha}|\delta\rangle \quad (40)$$

$$\left(U + 2J_c - K_c + J_o\right)|\gamma\rangle + \sum_{\delta}C_{\gamma\delta}|\langle\delta|V|\gamma\rangle\delta\rangle = \sum_{\beta}\epsilon_{\beta\gamma}|\beta\rangle + \sum_{\delta}\epsilon_{\delta\gamma}|\delta\rangle \quad (41)$$

where

$$|\langle\delta|V|\gamma\rangle\delta\rangle = \int d\vec{r}'\,\phi_\delta^*(\vec{r})\,V(\vec{r},\vec{r}')\,\phi_\gamma(\vec{r})\,\phi_\delta(\vec{r})$$

$$\langle W|V|W'\rangle = \int d\vec{r}'\,W^+(\vec{r})\,V(\vec{r},\vec{r}')\,W'(\vec{r}')$$

$$J_c = \sum_{\beta}\langle\beta|V|\beta\rangle \qquad J_o = \sum_{\delta}\langle\delta|V|\delta\rangle \quad (42)$$

$$K_c|W\rangle = \sum_{\beta}|\langle\beta|V|W\rangle\beta\rangle \qquad K_o|W\rangle = \sum_{\delta}|\langle\delta|V|W\rangle\delta\rangle$$

Left-multiplying Eq. (40) by $\langle\gamma|$ and Eq. (41) by $\langle\alpha|$, these equations can be combined to yield

$$\epsilon_{\gamma\alpha} = \sum_{\delta}(2C_{\gamma\delta} + 1)\langle\gamma\delta|V|\delta\alpha\rangle \quad (43)$$

Noting that

$$\sum_{\zeta} C_{\gamma\tau} \langle \delta\tau | v | \tau\gamma \rangle = \sum_{\tau} C_{\delta\tau} \langle \delta\tau | v | \tau\gamma \rangle, \tag{44}$$

Equations (40) and (41) can be recast as follows. From Eq. (40),

$$\frac{1}{2} \sum_{\delta} \epsilon_{\delta\alpha} | \delta \rangle = \frac{1}{2} M | \alpha \rangle$$

with

$$M = \sum_{\delta\tau} (2C_{\delta\tau} + 1) | \delta \rangle \langle \tau < \delta | v | \tau > | \tag{45}$$

From Eq. (41),

$$\sum_{\beta} \epsilon_{\beta\gamma} | \beta \rangle = \sum_{\beta\tau} (2C_{\gamma\tau} + 1) | \beta \rangle \langle \beta\tau | v | \delta\gamma \rangle = \mathcal{O}_c M^{+} | \gamma \rangle \tag{46}$$

with

$$\mathcal{O}_c = \sum_{\beta} | \beta \rangle \langle \beta | ; \quad \mathcal{O}_o = \sum_{\delta} | \delta \rangle \langle \delta | \tag{47}$$

Using Eqs. (46) and (47) in (40) and (41), we find

$$(U + 2J_c - K_c + J_o - \frac{1}{2} K_o - \frac{1}{2} M) | \alpha \rangle = \sum_{\beta} \epsilon_{\beta\alpha} | \beta \rangle \tag{48}$$

$$(U + 2J_c - K_c + J_o - \frac{1}{2} K_o + \frac{1}{2} M^{+} - \mathcal{O}_c M^{+}) | \gamma \rangle = \sum_{\delta} \epsilon_{\delta\gamma} | \delta \rangle \tag{49}$$

Finally, Eqs. (48) and (49) can be rearranged to yield the same Hermitian operator on the lhs with the resulting definition of the one-electron eigenenergies for the closed and open-shell eigenstates:

$$\epsilon'_\alpha = \langle \alpha | U + 2J_c - K_c + J_o - \tfrac{1}{2}K_o | \alpha \rangle \tag{50}$$

$$\epsilon'_\gamma = \langle \gamma | U + 2J_c - K_c + J_o - \tfrac{1}{2}K_o + \tfrac{1}{2}M^+ | \gamma \rangle \tag{51}$$

Equations (50) and (51) represent the correct one-electron energy expressions for the spin-projected eigenstate.

This formalism has been developed to extend the conventional HF method to include split-shell correlation and proper spin and symmetry projections. It has been incorporated into a computer program using Gaussian-type orbitals (GTO's) as the elementary basis functions. A crucial feature of this method is that dissociation always follows the lowest energy pathway thereby permitting a proper description of bond formation and breakage. In contrast, RHF or MC-SCF methods often exhibit improper dissociation character or exhibit size inconsistencies owing to correlation energy changes in going from molecular geometries to separated atom-molecule or atom-atom dimensions.

DISCUSSION OF RESULTS

Background

For several years, this Center has been involved in detailed ab initio quantum mechanical studies of the electronic structure, radiative and kinetic properties of diatomic and polyatomic molecules. These studies have focused on air molecules and metal oxides, with applications to weapons technology.

Our initial quantum mechanical studies dealt with the electronic structure and radiative lifetimes of the air system and certain diatomic metal oxide species which may be of abundance in the perturbed atmosphere following a thermonuclear explosion. These studies have included the systems NO, NO^+, NO_2, N_2O, TiO, and TiO^+. Such species commonly exhibit strong LWIR radiation and a quantitative measure of this effect is needed to analyze the atmospheric kinetics. These systems are of direct relevance to current DNA interests and to the general problem of identifying atmospheric kinetics and radiation properties. The studies were carried out using methods of molecular quantum mechanics coupled with available spectroscopic information on excited electronic states.

As a result of these investigations, which were mainly carried out under Air Force sponsorship, this Center has available a large data base of calculated electronic energies and transition probabilities for air system molecules (and molecular ions) and for metal oxide systems. This base includes calculations for the ground and many electronically excited states of these molecules. Several of these systems have been analyzed in detail (Refs. 65-75). To the best of our knowledge, no other laboratory in the country has such an extensive catalogue of theoretical calculations of the electronic structure of the air system and of the light metal oxides or our computational experience with these types of molecules. In addition, UTRC has fully developed sophisticated computer programs for studying both diatomic and polyatomic molecules. These programs have been extensively used at UTRC and at the Air Force computational laboratories at AFWL, Kirtland Air Force Base, and AFGL, Hanscom Field.

As a continuation of our theoretical research on atmospheric chemistry under the subject contract F19628-80-C-0209, we have examined the reaction kinetics for the ion-molecule reaction $O^+ + N_2 \rightarrow NO^+ + N$. A particular reaction which is very important in NO^+ formation is:

$$O^+\left[^4S\right] + N_2\left[X^1\Sigma_g^+\right] \rightarrow NO^+\left[X^1\Sigma^+\right] + N\left[^4S\right] \qquad (52)$$

$$\Delta E = -1.1\ ev$$

Another ion-molecule reaction whose role is less certain is:

$$O^+\left[^4S\right] + N_2^*\left[A^3\Sigma_u^+\right] \rightarrow NO^+\left[X^1\Sigma^+\right] + N\left[^4S\right] \qquad (53)$$

$$\Delta E = -7.3\ eV$$

Analysis of the kinetics of these reactions requires the calculation of the appropriate reaction surface or surfaces followed by a kinematic analysis of the motion of the reactants on such surfaces. In this work, we are primarily concerned with analysis of the $O^+ + N_2^{\ddagger}$ reaction (Eq. 52) in an energy region 0.1 → 10.0 eV, with this energy either as center-of-mass (CM) translational energy or as vibrational energy of the N_2 molecule. Our first concern, therefore, is to seek possible reaction paths which strongly couple reactants to products. We first examined states of quartet symmetry which exhibit allowed connections.

Potential Energy Surfaces

The molecular correlations that connect reactant to product states are given in Tables 1 and 2. The N_2O^+ correlation diagrams shown in Tables 1 and 2 list the reactant and product states in increasing energy and show the symmetry of the electronic states of N_2O^+ for collinear collision only. The lowest quartet state in a linear ($C_{\infty v}$) $O^+ - N_2$ conformation corresponds to $^4\Sigma^-$ symmetry. In Figs. 1 - 3, we show the adiabatic correlations for the quartet states of N_2O^+ in all possible symmetries, linear ($C_{\infty v}$), bent (C_s), and symmetric perpendicular (C_{2v}). In a bent geometry, the lowest potential energy surface has $^4A''$ symmetry but details of the energetics of this surface, to include possible avoided crossings with higher states, require accurate quantum mechanical calculations of the N_2O^+ molecular ion as a function of geometry. A limited region of this lowest potential energy surface can be described using a multipole expansion analysis for the long-range interactions as described below.

Long-Range Interactions

The long-range energy of interaction for this system can be conveniently represented in the natural coordinates for the collision as illustrated in Fig. 4. The collision angle β can be related to the molecular angle γ through use of the relations:

$$x = \left[R_{ON}^2 + \left(\frac{R_{NN}}{2}\right)^2 - R_{ON}\,R_{NN}\cos\gamma\right]^{1/2}$$

$$\sin\beta = \frac{R_{ON}}{x}\sin\gamma \qquad (54)$$

In terms of x and β, the long-range energy of interaction of $O^+ + N_2$ can be written as (Refs. 76 and 77):

$$V(O^+ + N_2) \underset{x\to\infty}{\simeq} + \frac{Q_{zz}(N_2)(3\cos^2\beta - 1)}{4x^3}$$

$$- \frac{(\alpha_{\parallel}(N_2)\cos^2\beta + \alpha_{\perp}(N_2)\sin^2\beta)}{2x^4} \qquad (55)$$

$$- \frac{3\alpha(O^+)(\alpha_{\parallel}(N_2)\cos^2\beta + \alpha_{\perp}(N_2)\sin^2\beta)}{2x^6(I^{-1}(O^+) + I^{-1}(N_2))}$$

The first term in Eq. (55) represents the ion-quadrupole interaction, the second term represents the main component of the energy of induction between the charge and the induced dipole and the third term is the London dispersion energy based on the approximate Drude formula. A small contribution (x^{-8}) to the energy of induction has been neglected owing to the smallness of the permanent moments for this system.

In the product channel, the long-range energy of interaction of $N + NO^+$ can be written as

$$V(N + NO^+) \underset{x\to\infty}{\simeq} - \frac{\alpha(N)}{2x^4} - \frac{3\alpha(N)(\alpha_{\parallel}(NO^+)\cos^2\bar{\beta} + \alpha_{\perp}(NO^+)\sin^2\bar{\beta})}{2x^6(I^{-1}(N) + I^{-1}(NO^+))} \qquad (56)$$

where $\bar{\beta}$ refers to the corresponding collisional angle measured in the product channel framework. Note that the ion-quadrupole interaction vanishes here since the N atom is in a ^4S state.

In Table 3, we give values for the parameters appearing in Eqs. (55) and (56). Since dipole polarizabilities for the ions are not available, they are estimated from the corresponding neutral species using expectation values, $\overline{r_i^2}$, calculated from corresponding neutral and ionic Hartree-Fock wavefunctions.

Values of the long-range interactions calculated from Eqs. (55) and (56) are presented in Tables 4 and 5, respectively. Comparison with interaction potentials derived from an MC-SCF calculation (Ref. 78) indicates significant differences. This suggests an inaccurate representation of polarization forces using this MC-SCF wavefunction.

Ab Initio Calculations

The first ab initio calculations for the N_2O^+ system are those reported by Pipano and Kaufman (Refs. 79 and 80) for a collinear arrangement of the nuclei. These results were obtained using an atom-optimized minimum Slater-type orbital (STO) basis with a very large configuration-interaction (CI) constructed by including all single and double electron excitations from the ground reference state. The final CI sizes (1379 for $^4\Pi$ symmetry and 1310 for $^4\Sigma^-$ symmetry) represented pioneering work for a molecular system of this complexity. Pipano and Kaufman found that both the $^4\Pi$ and $^4\Sigma^-$ channels lie too high in energy to permit a direct reaction mechanism from $O^+ + N_2$ to $NO^+ + N$. Instead, they postulated that this reaction must involve multi-surface mechanisms involving the crossings: $^4\Sigma^- \rightarrow {}^2\Pi \rightarrow {}^4\Sigma^-$ or possibly $^4\Sigma^- \rightarrow {}^4\Pi \rightarrow {}^4\Sigma^-$. As we shall see below, for low collisional energies (< 0.1 eV), the multi-surface reaction of Pipano and Kaufmann is the most probable mechanism but the experimental evidence supports a direct reaction mechanism for higher collisional energies.

A limited study of bent conformations of N_2O^+ was also reported by Pipano and Kaufman but an unfortunate choice of the bending angle (5° relative to a linear conformation) led them, as we shall see, to the incorrect conclusion that the energy increased with bending the molecule.

Extensive ab initio SCF and MC-SCF studies of the lowest potential surface of N_2O^+ have been reported by Hopper (Refs. 81 and 82). Hopper found that a bent conformation of the nuclei for N_2O^+ resulted in a significant lowering of the energy from the collinear arrangement studied by Pipano and Kaufman. He reports a saddle point, with a barrier height of 2.6 eV, in the lowest $^4A''$ surface at the geometry: R_{NN} = 2.42 bohrs, R_{NO} = 2.38 bohrs, $\angle$ NNO = 120°. These bond lengths represent an expansion from the equilibrium values for NO^+ (2.0092 bohrs) and N_2 (2.0742 bohrs). In another study (Ref. 78), Hopper reports calculations on the lowest $^4\Sigma^-$ surface resulting from a collinear arrangment of the nuclei. Again, he finds a saddle region at considerably expanded bond lengths (R_{NN} = 2.8 bohrs, R_{NO} = 2.6 bohrs) and a calculated barrier height of $\sim$ 8.0 eV relative to the $O^+ + N_2$ asymptote.

Both of these surfaces exhibit barrier heights that are much too large to explain the experimentally known energy dependence of the

$O^+ + N_2 \rightarrow NO^+ + N$ reaction. Hopper argues (Ref. 82) that a complicated reaction coordinate begining with a polarization $^4\Sigma^-$ state and switching to a bent conformation at the saddle point yields a reaction path that has a barrier less than $\sim$ 0.2 eV. Such a value would be in accord with the best experimental evidence. His argument for this low barrier height, however, is not based on his calculated value (2.6 eV) but rather on a circumlocutory thermodynamic cycle argument involving a mix of calculated, experimental and estimated data. It was felt, therefore, that a re-examination of the lowest potential surface for N_2O^+ should be carried out.

Open-Shell Ab Initio Calculations

Our initial studies were directed toward an examination of the lowest $^4\Sigma^-$ and $^4\Pi$ surfaces of N_2O^+ using a large CI and employing accurate Slater-type orbit (STO) basis sets. This Center has operational a very sophisticated computer code for polyatomic calculations which incorporates these features. Both single-zeta (minimum basis) and contracted double-zeta STO basis were examined. In either case, a complete CI represents 1488 configurations for $^4\Sigma^-$ and 531 configurations for $^4\Pi$. These CI expansions include all possible orbital occupancies and all possible spin coupling among the valence electrons.

Previous studies in this Center on N_2O^+ (Ref. 83) had shown that SCF or MC-SCF calculations may exhibit artifically high reaction barriers in $C_{\infty v}$ symmetry. The origin of the problem is that SCF or MC-SCF methods generally employ maximum pairing in their MO structure and thus impose constraints on spin-recoupling that may occur along the reaction coordinate. The SCF structure of $N_2O^+[^4\Sigma^-]$ can be written as

$$^4\Sigma^- = 1\sigma^2 2\sigma^2 3\sigma^2 4\sigma^2 5\sigma^2 6\sigma^2 1\pi^4 7\sigma^2 2\pi^2 8\sigma \qquad (57)$$

where at short $O^+ - N_2$ separations, corresponding to product ion formation, we can identify the principal AO composition of these MO's as follows:

$$\begin{aligned} 1\sigma, 2\sigma, 3\sigma &= 1s \\ 4\sigma &= 2s_O \\ 5\sigma &= 2s_N(\text{outer}) \\ 6\sigma &= 2s_N(\text{inner}) \\ 7\sigma &= 2p\sigma(NO^+) \\ 8\sigma &= 2p\sigma_N(\text{outer}) \\ 9\sigma &= 2p\sigma^*(NO^+) \\ 1\pi &= 2p\pi\ (NO^+) \\ 2\pi &= 2p\pi_N\ (\text{inner}) \\ 3\pi &= 2p\pi^*\ (NO^+) \end{aligned} \qquad (58)$$

At large $O^+ - N_2$ separations, the MO composition for the 2p electrons must be:

$$\begin{aligned} 7\sigma &= 2p\sigma(N_2) \\ 8\sigma &= 2p\sigma(O^+) \\ 1\pi &= 2p\pi(N_2) \\ 2\pi &= 2p\pi(O^+) \end{aligned} \tag{59}$$

Thus both the σ and π orbitals are completely recoupled spin-wise in going from $O^+ + N_2$ to $N + NO^+$. In Fig. 5, we present a general vector coupling diagram which indicates that there are 48 separate spin-states for nine electron quartet couplings. The reaction $O^+ + N_2 \rightarrow NO^+ + N$ involves a complete spin-recoupling as the pairing changes in going from reactants to products, which suggests that a valence bond treatment is more appropriate than SCF or limited MC-SCF expansions. Previous studies on the much simpler H_3 surface have indicated the importance of including higher spin-coupled states (Ref. 84).

Preliminary studies were carried out under AFGL Contract F19628-77-C-0248 which confirm that the spin-recoupling that occurs in going from reactants to products is not adequately represented within SCF or limited MC-SCF frameworks. A calculation for the lowest $^4\Sigma^-$ state of N_2O^+ at intermediate internuclear separations yields a spin-correlation error of 6 eV. This value closely corresponds to the 8 eV barrier found in the MC-SCF calculations by Hopper (Ref. 78). The major error arises from the 7σ and 1π molecular orbitals which change in composition from primarily N_2 in character at large $O^+ + N_2$ separations (reactants), to mainly NO^+ at large $N + NO^+$ separations. This error corresponds to 2 eV/electron pair, a value that is typical of many atomic and molecular systems.

A second problem with limited extent MC-SCF calculations is size inconsistency errors arising from changes in the correlation energy in going from N_2O^+ to $O^+ + N_2$ ($NO^+ + N$) and to the ($O^+ + N + N$) separated atom limits. The SCF wavefunction given in Eq. (57) dissociates properly in both the $O^+ + N_2$ and $NO^+ + N$ limits but is incapable of proper description of the plateau dissociation to $O^+ + N + N$. In this region, the minimum CI (or MC-SCF) must include:

$[1\sigma^2 \ldots 6\sigma^2]$ | $7\sigma^2\ 8\sigma\ 1\pi_x^2\ 1\pi_y^2\ 2\pi_x\ 2\pi_y$ Conf.: (1)

| $7\sigma^2\ 8\sigma\ 1\pi_x^2\ 3\pi_y^2\ 2\pi_x\ 2\pi_y$ (2)

| $7\sigma^2\ 8\sigma\ 3\pi_x^2\ 1\pi_y^2\ 2\pi_x\ 2\pi_y$ (3)

| $7\sigma^2\ 8\sigma\ 3\pi_x^2\ 3\pi_y^2\ 2\pi_x\ 2\pi_y$ (4)

| $9\sigma^2\ 8\sigma\ 1\pi_x^2\ 1\pi_y^2\ 2\pi_x\ 2\pi_y$ (5)

| $9\sigma^2\ 8\sigma\ 1\pi_x^2\ 3\pi_y^2\ 2\pi_x\ 2\pi_y$ (6)

| $9\sigma^2\ 8\sigma\ 3\pi_x^2\ 1\pi_y^2\ 2\pi_x\ 2\pi_y$ (7)

| $9\sigma^2\ 8\sigma\ 3\pi_x^2\ 3\pi_y^2\ 2\pi_x\ 2\pi_y$ (8)

The first configuration is the basic SCF representation and the others are those required for correct atomic limit behavior. Hopper (Ref. 78) has included configurations (1), (2), (3), and (5) [his (1), (2), (3), and (13)] in his MC-SCF construction for the lowest $^4\Sigma^-$ state but these are insufficient for proper atomic dissociation. As a result, it is predictable that his MC-SCF calculations will exhibit increasing correlation errors for N_2O^+ geometries tending toward $O^+ + N + N$ dissociation. Thus the saddle region (extended N-N and N-O bonds) will be poorly described relative to $O^+ + N_2$ ($NO^+ + N$) using Hopper's MC-SCF construction. This is borne out by his calculated energy for the saddle point on the $^4\Sigma^-$ surface. His reported energy at the barrier is -183.160 hartrees, a value already equal to the atomic dissociation limit (-183.159998) with his basis set. Hopper's predicted location and energetics of the barrier region must therefore reflect this correlation dissociation error.

The results of our CI-STO basis calculations for $^4\Sigma^-$ symmetry predict a saddle point at $R_{NN} \sim R_{NO} \sim 2.2$ bohrs with a barrier height of 0.1363 hartrees (3.7 eV) relative to the asymptote of $O^+ + N_2$. This CI consisted of a full expansion of all σ and π valence space of N_2O^+ and included all eight configurations listed above. Based on this result, we concluded that a linear conformation of nuclei is not the lowest possible quartet surface for N_2O^+.

A similar CI-STO basis calculation was carred out for $^4\Pi$ symmetry. At $R_{NN} = R_{ON} = 2.0$ bohrs, the lowest $^4\Pi$ state lies 0.1509 hartrees above the $O^+ + N_2$ asymptote, very close to the $^4\Sigma^-$ surface. This state has a dominant configuration that can be represented as

$$^4\Pi\ [1\sigma^2\ \ldots\ 6\sigma^2\ 7\sigma^2\ 1\pi^3\ 2\pi^3\ 3\pi] \qquad (60)$$

At shorter $O^+ - N_2$ separations, the dominant configuration switches to

$$^4\Pi\ [1\sigma^2\ \ldots\ 6\sigma^2\ 7\sigma^2\ 1\pi^4\ 2\pi^2\ 3\pi] \qquad (61)$$

and at large $O^+ - N_2$ separations, the dominant configuration is

$$^4\Pi\ [1\sigma^2\ \ldots\ 6\sigma^2\ 7\sigma\ 8\sigma\ 1\pi^4\ 2\pi^3]\ . \qquad (62)$$

Thus a complicated crossing of the $^4\Pi$ surfaces occurs between R_{N-O} = 2.0 - 3.0 bohrs. However, none of these linear surfaces is low enough to explain the observed energy dependence of this reaction.

The results of these linear conformation studies led us to examine the lowest $^4A''$ surface at several internuclear separations and bond angles. Owing to cost and time considerations, the $^4A''$ surface was studied in a projected UHF framework using Gaussian-type orbitals (GTO's) in single-ζ, double-ζ and double-ζ + single d-polarization function approximations. The latter two expansions were checks on the work of Hopper (Refs. 78 and 82). After much experimentation, it became clear that the minimum energy reaction path lies close to a 45° trajectory of $O^+ + N_2$ as illustrated in Fig. 4. Of course, all possible trajectories from $\lambda = 0 \rightarrow \lambda = 90°$ will be traversed, but only those near the 45° channel lead to the reactive rearrangement collision: $O^+ + N_2 \rightarrow NO^+ + N$.

To insure a systematic comparison, the linear surfaces for the lowest $^4\Sigma^-$ and $^4\Pi$ states were recalculated within the UHF approximation. They are given in Table 6 and illustrated in Fig. 6. Our calculated barrier for the lowest $^4\Sigma^-$ surface is 0.128 hartrees (3.5 eV), close to the value found for the CI-STO basis calculations. A lower linear reaction pathway involves a $^4\Pi - {}^4\Sigma^-$ surface crossing at an energy of $\sim$ 0.11 hartrees (3.0 eV), a value still too high to explain the collisional data. A comparison of the several ab initio calculations of the lowest $^4\Sigma^-$ surface is shown in Fig. 7. We have also included the analytical long-range potential for comparison with the previous studies of Pipano and Kaufman (Ref. 80) and Hopper (Ref. 78). In general, Pipano and Kaufman's CI-STO results tend to over-emphasize the long-range behavior whereas Hopper's MC-SCF results exhibit an unbalance in their long-range behavior. The excess long-range attraction exhibited by Hopper's calculation in the $O^+ + N_2$ channel is most probably a reflection of an unbalance in errors in his calculations for N_2 [$X^1\Sigma_g^+$] (2.03 eV error in D_e) and NO^+ [$X^1\Sigma^+$] (3.79 eV error in D_e). The extra attraction in the $O^+ + N_2$ reactant channel and the extra repulsion in the $NO^+ + N$ product channel are a reflection of these asymptotic errors in going from the reactants $O^+ + N_2$ to N_2O^+ and finally to products $NO^+ + N$. However, all calculations clearly illustrate that linear surfaces cannot explain the energy dependence of this reaction.

As mentioned above, our lowest energy reaction path closely follows a 45° trajectory. An optimization of the saddle region along this path was carried out. This reaction surface is in a convenient coordinate framework for collisional studies but differs from conventional studies which use the bond angle of the molecule as an independent surface geometry parameter. Our constant trajectory angle of 45° corresponds to a cut through many surfaces with the molecular bond angle changing from about 115 → 120°. The lowest energy reaction path is given in Table 7 and is illustrated in Fig. 8. We find a barrier height of ∿ 0.01 hartrees (0.3 eV) and a relatively flat surface in the region: $3.4 < x < 3.8$ bohrs. Also shown in Fig. 8 is the reaction path calculated by Hopper (Ref. 82) within a restricted HF-SCF framework and at a constant molecular angle of 120°. This translates to a collisional angle varying from about 40 → 45°, close to our optimum trajectory. Hopper's basic conclusion that the lowest energy quartet surface for N_2O^+ is bent is thus confirmed by these studies. The $O^+ + N_2 \rightarrow NO^+ + N$ reaction would appear to take place on a single hypersurface for collisional energies between ∿ 0.1 and several electron volts, namely for collisional energies sufficient to cross the barrier in the lowest "A" surface.

Potential Surface Modeling

There are several approaches that can be taken to yield a functional representation of the reaction potential energy surface. The ab initio calculations produce a large table of numbers that must somehow be fitted and smoothed for use in trajectory calculations of reaction rates. Our first approach was to examine an expansion of the interaction potential between O^+ and N_2 in terms of Legendre polynominals as

$$V(R, x, \lambda) = \sum_{\substack{l=0 \\ \text{even}}} V_l(R, x)\, P_l(\cos \lambda) \tag{63}$$

This form has been examined previously for $Li^+ + H_2$ (Ref. 85) and $H^- + H_2$ (Ref. 86) collisional studies. An analysis of the lowest $^4A''$ surface of N_2O^+ in terms of Eq. (63) yields a slowly convergent expansion owing to complications of representing both the attractive long-range potential for linear $O^+ + N_2$ and the relatively flat saddle region for $\lambda = 45°$. Thus the utility of employing Eq. (63) rather than a direct table interpolation scheme seems questionable.

An alternate approach is to choose a more restricted functional form than that represented by Eq. (63) but one that can easily incorporate the known asymptotic behavior of the system at the $O^+ + N_2$ and $NO^+ + N$ limits. The London-Eyring-Polanyi-Sato (LEPS) model (Ref. 87) has been very successful in applications to atom-molecule collisions (Ref. 88). For the N_2O^+ system, the three-body interaction potential can be written as

$$V_{abc} = \rho\left[Q_{ab} + Q_{bc} + Q_{ca}\right]$$

$$- \frac{1-\rho}{\sqrt{2}}\left[(\alpha_{ab} - \alpha_{bc})^2 + (\alpha_{bc} - \alpha_{ac})^2 + (\alpha_{ac} - \alpha_{ab})^2\right]^{1/2} \quad (64)$$

where Q_{ij} and α_{ij} are the Coulomb and exchange two-body interactions and ρ is treated as an empirical parameter. The Q_{ij} and α_{ij} are related to the diatomic potential functions by

$$V_{ij} = Q_{ij} + \lambda\alpha_{ij} \quad (65)$$

where the V_{ij} can be expressed by some empirical form such as a Morse function (Ref. 89). For these present studies, Eq. (65) was fitted to a Hulbert-Hirschfelder potential function (Ref. 90) modified to include the long-range polarization tail. The adjustable parameters were used to fit Eq. (64) in critical regions of the potential surface such as the barrier and asymptotic regions. The fitted minimum energy LEPS reaction path is close to the UHF surface in the region of the saddle point as can be seen in Fig. 8.

In Figs. 9 and 10, we give the LEPS representation for the N_2O^+ surface in C_{2v} symmetry. Figure 10 illustrates the large barrier for reaction in this geometry. The collinear LEPS surface is shown in Fig. 11 which again illustrates a large reaction barrier. A LEPS surface cut at a fixed molecular angle of 120° is shown in Figs. 12 and 13. The barrier height is much reduced for this bent geometry. Finally, in Fig. 14, we show the minimum energy reaction surface that was employed in the collisional studies. An important feature of this surface is that the saddle point is nearly symmetrically located between the entrance and exit channels. Thus either translational or vibrational energy should be effective in this reaction. Translation energy is effective in surmounting the barrier while vibrational energy is effective is converting to $NO^+ + N$ products in the exit channel. A barrier region deep in either the entrance or exit channels would exhibit bias toward translational or vibrational energy, respectively. The surface represented by Fig. 14 is that employed in the collisional studies described below.

Kinetics of the $O^+ + N_2$ Reaction

Our kinetic studies were restricted to the analysis of the reaction

$$O^+\left[^4S\right] + N_2^{\ddagger}(V)\left[X\,^1\Sigma_g^+\right] \rightarrow NO^+\left[X\,^1\Sigma_g^+\right] + O\left[^4S\right] \quad (66)$$

in the energy region $0.1 < KE_{cm} < 10.0$ eV. For energies below $\sim$ 0.1 eV, the rate coefficient for the reaction shown in Eq. (66) is very small ($\sim 10^{-12}$ cm^3/sec) compared to the Langevin rate and exhibits a negative energy dependence (Refs. 91-95). A mechanism for this low energy behavior was first discussed by Ferguson (Ref. 93) and, more recently, by Pipano and Kaufman (Ref. 80) and Hopper (Ref. 82).

Using our minimum energy $^4A''$ potential surface ($\lambda = 45°$), calculations of the cross-section for reaction (66) were carried out employing the R-matrix propagator technique (Ref. 62). For each value chosen for the collision energy, a sum over all allowed j states was carried out to convergence. For the range of collision energies considered here ($0.1 < KE_{cm} < 10.0$ eV), this sum converged for the off-diagonal elements of the S-matrix for $j < 400$. The effect of increased vibrational energy in the N_2 molecule was studied by analyzing the collisions occurring higher up along the reaction surface in the $O^+ + N_2$ entrance channel.

Our calculated reaction cross-sections are given in Table 8 and illustrated in Fig. 15. We see that increasing either the translational energy of the collision or the vibrational energy of the N_2 molecule results in a dramatic increase in the reaction cross-section at low energies. For comparison, the Langevin rate (Refs. 96 and 97), which is determined by long-range orbiting collisions, is shown for comparison. We see that the Langevin rate is totally inaccurate both in magnitude and energy dependence in this energy range. The physical effect that gives rise to our calculated energy dependence is the presence of the barrier in the reaction channel which cuts off the cross section for $E \lesssim 0.1$ eV. The experimental cross section has been measured by Kaneko and Kobayashi (Ref. 95) for $E < 0.5$ eV where it eventually turns around and begins to increase as the energy is further decreased, reflecting the curve-crossing mechanism (Ref. 93) governing the very low energy behavior of this reaction. The experimental beam data of Giese (Ref. 91) are also shown in Fig. 15. The overall agreement with our ground vibrational state curve is excellent.

A more direct comparison can be made for the energy dependence of the reaction rate constant. Using an averaged velocity given by

$$V_{rel} = \left[\frac{2E_{cm}}{\mu}\right]^{1/2} \tag{67}$$

the reaction rate constants have been calculated as a function of the vibration levels of N_2. These calculated rate constants are given in Table 9 and are illustrated in Fig. 16. The experimental data of the NOAA group and others (Refs. 98 and 99) are shown for comparison. The discrepancy for $E \lesssim 0.2$ eV is again due to the fact that we have not included in our analysis the dominant curve-crossing mechanism for these low energy collisions.

A direct comparison of the relative roles of vibrational and translational energy is shown in Fig. 17 where the vibrational energy has been incorporated into an equivalent total energy for the reactant channel. It is apparent that no significant differences arise from the distribution of the total energy into a vibrational rather than a translational mode. The data of Schmeltekopf et al. (Ref. 100) are shown for comparison, where the relationship $E_{vib} = 3/2(kT_{vib})$ has been used. Again, the discrepancy below $\sim$ 0.2 eV arises from the absence of the dominant low energy curve-crossing mechanism from our analysis.

A semi-empirical model for the vibrational dependence of the $O^+ + N_2$ reaction has been proposed by O'Malley (Ref. 101). This model predicts that vibrational excitation of the N_2 molecule should affect the rate constant much more strongly than the kinetic energy of the collision. This is in disagreement with both experiment and our calculations, but the overall qualitative behavior (increase with v) of the rate constant is exhibited by O'Malley's model.

Finally, we examine the reaction:

$$O^+\left[^4S\right] + N_2\left[A\,^3\Sigma_u^+\right] \rightarrow N_2O^+ \rightarrow \text{products} \qquad (68)$$

As indicated in Fig. 2, this reaction can begin on the surfaces $^2A''$, $^4A''$ and $^6A''$ in the general bent geometry conformation. However, these excited hypersurfaces surely exhibit crossing with surfaces of the same symmetry that lie at lower energies. Thus, the reaction given by Eq. (68) may start on the adiabatic surface shown in Fig. 2 but the reaction diabatically can connect to several different product channels. This situation is in contrast to the ground state reaction which has only one accessible potential energy surface for low energy collisions. The reaction given by Eq. (68) should therefore proceed at near Langevin rate unless an activation barrier is present early in the reactant channel. Detailed _ab initio_ studies of this hypersurface would appear to be very complex and time consuming since the adiabatic channel, for example, is represented by the eighth excited state for $^4A''$ symmetry.

In summary, the $O^+ + N_2 \rightarrow NO^+ + N$ reaction has been shown to take place on the lowest $^4A''$ hypersurface for this system, for collisional energies greater than about 0.1 eV. This confirms the earlier results reported by Hopper that a bent configuration of the nuclei exhibits the lowest energy for this system. A small barrier, located symmetrically between the entrance and exit channels, gives rise to the experimentally observed energy dependence for this reaction for $KE_{cm} > 0.1$ eV. The energy dependence is also shown to be nonspecific, either vibrational or translational energy is effective in promoting the

reaction. Finally the very low energy behavior (KE_{cm}<.1 eV) of this reaction must be controlled by a separate reaction mechanism involving hypersurface crossings and weak spin-orbit coupling as first proposed by Ferguson (Ref. 93). For such low collisional energies, the barrier in the $^4A''$ surface prevents direct charge rearrangement collision from occurring and an indirect mechanism, based on doublet-quartet surface crossings, must come into play.

REFERENCES

1. Harang, O.: A10 Resonant Spectrum for Upper Atmosphere Temperature Determination. AFCRL-66-314, Environmental Research Paper, No. 192, 1966.

2. Churchill, D. R. and R. E. Meyerott: "Spectral Absorption in Heated Air," Journal of Quantitative Spectroscopy and Radiative Transfer, Vol. 5, p. 69, 1965.

3. The Airglow and the Aurorae, edited by E. B. Armstrong and A. Dalgarno. Pergamon Press, New York, 1955.

4. Armstrong, B. H., R. R. Johnston and P. S. Kelly: "The Atomic Line Countribution to the Radiation Absorption Coefficient of Air," Journal of Quantitative Spectroscopy and Radiative Transfer, Vol. 5, p. 55, 1965.

5. Johnston, R. R., B. H. Armstrong and O. R. Platas: "The Photoionization Contribution to the Radiation Absorption Coefficient of Air," Journal of Quantitative Spectroscopy and Radiative Transfer, Vol. 5, p. 49, 1965.

6. Harris, F. E. and H. H. Michels: "Open-Shell Valence Configuration - Interaction Studies of Diatomic and Polyatomic Molecules," International Journal of Quantum Chemistry, Vol. IS, p. 329, 1967.

7. Krauss, M.: Compendium of ab initio Calculations of Molecular Energies and Properties. NBS Technical Note 438, December 1967.

8. McLean, A. D. and B. Liu: "Classification of Configurationsand the Determination of Interacting and Noninteracting Spaces in Configuration Interaction," Journal of Chemical Physics, Vol. 58, p. 1066, 1973.

9. Schaefer, H. F.: Electronic Structure of Atoms and Molecules. Addison-Wesley Publishing Co., 1972.

10. Neynaber, R. H. and G. D. Magnuson: "Low Energy Study of $O + N_2 \rightarrow NO^+ + N$," Journal of Chemical Physics, Vol. 58, p. 4586, 1973.

11. Rutherford, J. A., R. H. Neynaber, and D. A. Vroom: Measurements of Selected Charge Transfer Processes at Low Energies. IRT Corporation Final Report (IRT 8163-007) Defense Nuclear Agency Report No. DNA 4695F, 1978.

12. Michels, H. H.: Theoretical Research Investigation Upon Reaction Rates to the Nitric Oxide (Positive) Ion. Interim Scientific Report (AFGL-TR-79-0190) for AFGL Contract F19628-77-C-0248, July 1979.

13. Michels H. H.: Theoretical Research Investigation Upon Reaction Rates to the Nitric Oxide (Positive) Ion. Final Report (AFGL-TR-80-0072) for AFGL Contract F19628-77-C-0248, January 1980.

14. Allen, L. C.: Quantum Theory of Atoms, Molecules and the Solid State, Edited by P. O. Löwdin, Academic Press, Inc., New York, 1966.

15. Roothan, C. C. J. and P. S. Bagus: "Atomic Self-Consistent Field Calculations by the Expansion Method, "Methods in Computational Physics, Edited by B. Alder, Vol. 2, p. 47, 1963.

16. Roothan, C. C. J.: "New Developments in Molecular Orbital Theory," Reviews of Modern Physics, Vol. 23, No. 2, April 1951, p. 69.

17. Harris, F. E.: "Molecular Orbital Studies of Diatomic Molecules. 1. Method of Computation for Single Configurations of Heteronuclear Systems," Journal of Chemical Physics, Vol. 32, p. 3, 1960.

18. Harris, F. E.: "Open-Shell Orthogonal Molecular Orbital Theory," Journal of Chemical Physics, Vol. 46, p. 2769, 1967.

19. Givens, W.: Eigenvalue-Eigenvector Techniques, Oak Ridge Report Number ORNL 1574 (Physics).

20. Shavitt, I., C. F. Bender, A. Pipano, and R. P. Hosteny: "The Iterative Calculation of Several of the Lowest or Highest Eigenvalues and Corresponding Eigenvectors of Very Large Symmetric Matrices," Journal of Computational Physics, 11, p. 90, 1973.

21. Schaefer, F. E. and F. E. Harris: "Ab Initio Calculations of 62 Low-Lying States of the O_2 Molecule," Journal of Chemical Physics, Vol. 8, p. 4946, 1968.

22. Michels, H. H. and F. E. Harris: Predissociation Effects in the A $^2\Sigma^+$ State of the OH Radical," Chemical Physics Letters, Vol. 3, p. 441, 1969.

23. Harris, F. E. and H. H. Michels: "The Evaluation of Molecular Integrals for Slater-Type Orbitals," Advances in Chemical Physics, Vol. 13, p. 205, 1967.

24. Davidson, E. R.: "Natural Expansion of Exact Wavefunctions, III. The Helium Atom Ground State," Journal of Chemical Physics, Vol. 39, p. 875, 1963.

25. Wahl, A. C., P. J. Bertoncini, G. Das and T. L. Gilbert: "Recent Progress Beyond the Hartree-Fock Method for Diatomic Molecules. The Method of Optimized Valence Configurations," International Journal of Quantum Chemistry. Vol. IS, p. 123, 1967.

26. For a review article on this method, see J. C. Slater, Advance in Quantum Chemistry, 6, 1, 1972.

27. Lowdin, P. O.: "Quantum Theory of Many-Particle Systems. I. Physical Interpretations by Means of Density Matrices, Natural Spin-Orbitals, and Convergence Problems in the Method of Configuration Interaction," Physical Review, Vol. 97, p. 1474, 1955.

28. Kohn, W. and L. Sham: "Self-Consistent Equations Including Exchange and Correlation Effects," Physical Review, Vol. 140A, p. 1133, 1965.

29. Slater, J. C.: "A Simplification of the Hartree-Fock Method,: Physical Review, Vol. 81, p. 385, 1951.

30. Schwarz, K.: "Optimization of the Statistical Exchange Parameters α for the Free Atoms H through Nb," Physical Review, Vol. B5, p. 2466, 1972.

31. Beebe, N. H. F.: "On the Transition State in the X_α Method," Chemical Physics Letters, Vol. 19, p. 290, 1973.

32. Schwarz, K. and J. W. D. Connolly: "Approximate Numerical Hartree-Fock Method for Molecular Calculations," Journal of Chemical Physics, Vol. 55, p. 4710, 1971.

33. Connolly, J. W. D.: unpublished results.

34. Slater, J. C.: "Hellmann-Feynman and Virial Theorems in the X_α Method," Journal of Chemical Physics, Vol. 57, p. 2389, 1972.

35. Michels, H. H., R. H. Hobbs and J. C. Connolly: "Optimized SCF-X_α Procedures for Heterpolar Molecules," Journal of Chemical Physics (to be published, 1982).

36. Rosch, Notker and Keith H. Johnson: "On the Use of Overlapping Spheres in the SCF-X_α Scattered-Wave Method," Chemical Physics Letters, Vol. 23, p. 149, 1973.

37. Aaron, R., R. Amado and B. Lee: "Divergence of the Green's Function Series for Rearrangement Collisions," Physical Review, Vol. 121, p. 319, 1961.

38. Bates, D. R. and R. McCarroll: "Charge Transfer," Advances in Physics, Vol. 11, p. 39, 1962.

39. Bates, D. R. and R. McCarroll: "Electron Capture in Slow Collisions," Royal Society of London Proceedings, Vol. A245, p. 175, 1958.

40. Bates, D. R. and D. A. Williams: "Low-Energy Collisions Between Hydrogen Atoms and Protons," Physical Society Proceedings, Vol. A83, p. 425, 1964.

41. Fulton, M. J. and M. H. Mittleman: "Scattering of H^+ by H," Annals of Physics, Vol. 33, p. 65-76, 1965.

42. Quong, J.: Approximations in the Theory of Rearrangement Collisions and Applications to a Tractable Model of Charge-Exchange Scattering, Lawrence Radiation Laboratory Report UCRL-17034, August 19, 1966.

43. Riley, M. E.: "Strong-Coupling Semiclassical Methods. The Average Approximation for Atom-Atom Collisions," Physical Review A, Vol. 8, p. 742, 1973.

44. Massey, H. S. W. and R. A. Smith: Royal Society of London Proceedings, Vol. A126, p. 259, 1930.

45. Dalgarno, A. and R. McCarroll: "Adiabatic Coupling Between Electronic and Nuclear Motion in Molecules," Royal Society of London Proceedings, Vol. A237, p. 383, 1956.

46. Hahn, Y.: "Distorted Cluster States in Scattering Theory," Physical Review, Vol. 154, p. 981, 1967.

47. Marchi, R. P. and F. T. Smith: "Theory of Elastic Differential Scattering in Low-Energy He^+ + He Collisions," Physical Review, Vol. 139, p. A1025, 1965.

48. Smith, F. J.: "The Probability of Electron Capture at Fixed Scattering Angles in H^+ - H Collisions," Physical Society Proceedings, Vol. 84, p. 889, 1964.

49. Dalgarno, A.: "Spin-Exchange Cross Sections," Royal Society of London Proceedings, Vol. 262A, p. 132, 1961.

50. Kolker, H. J. and H. H. Michels: "Elastic Scattering Diffusion and Excitation Transfer of Metastable Helium in Helium," Journal of Chemical Physics, Vol. 50, p. 1762, 1969.

51. Schneiderman, S. B. and H. H. Michels: "Quantum-Mechanical Studies of Several Helium-Lithium Interaction Potentials," Journal of Chemical Physics, Vol. 42, p. 3706, 1966.

52. Michels, H. H.: "Molecular Orbital Studies of the Ground and Low-Lying Excited States of the HeH^+ Molecular Ion," Journal of Chemical Physics, Vol, 44, p. 3834, 1966.

53. Schneiderman, S. B. and A. Russek: "Velocity-Dependent Orbitals in Proton-On-Hydrogen Atom Collisions," Physical Review, Vol. 181, p. 311, 1969.

54. Thorson, W. R.: "Theory of Slow Atomic Collisions I. H_2^+," Journal of Chemical Physics, Vol. 42, p. 3878, 1965.

55. Kouri, D. J. and C. F. Curtiss: "Phase Shifts and the Quantum-Mechanical Hamilton-Jacobi Equation," Journal of Chemical Physics, Vol. 43, p. 1919, 1965.

56. Zemach, C.: "Phase-Shift Equations for Many Channel Problems," Nuovo Cimento, Vol. 33, p. 939, 1964.

57. Kouri, D. J. and C. F. Curtiss: "Low-Energy Atomic Collisions I. The Schrödinger Equation for H^+-H," Journal of Chemical Physics, Vol. 44, p. 2120, 1966.

58. Mittleman, M. H.: "Proton-Hydrogen Scattering System," Physical Review, Vol. 122, p. 499, 1961.

59. Bates, D. R. and A. R. Holt: "Impact Parameter and Semiclassical Treatments of Atomic Collisions," Physical Society Proceedings, Vol. 85, p. 691, 1965.

60. Marcus, R. A.: "Analytical Mechanics of Chemical Reactions. III. Natural Collision Coordinates," Journal of Chemical Physics, Vol. 49, p. 2610, 1968; On the Analytical Mechanics of Chemical Reactions. Quantum Mechanics of Linear Collisions, ibid, Vol. 45, p. 4493, 1966.

61. Stechel, E. B., T. G. Schmalz and J. C. Light: "Quantum Theory of Exchange Reactions: Use of Nonorthogonal Bases and Coordinates," Journal of Chemical Physics, Vol. 70, p. 5640, 1979.

62. Diestler, D. J.: "Close-Coupling Techniques for Chemical Exchange Reaction of the Type $A + BC \rightarrow AB + C$, $H + H_2 \rightarrow H_2 + H^*$," Journal of Chemical Physics, Vol. 54, p. 4547, 1971.

63. Pople, J. A. and R. K. Nesbet: "Self-Consistent Orbitals for Radicals", Journal of Chemical Physics, 22, p. 571, 1954.

64. Nesbet, R. K.: "Approximate Methods in the Quantum Theory of Many-Fermion Systems", Reviews of Modern Physics, 33, p. 28, 1961.

65. Michels, H. H. and H. P. Broida: "Analysis of the Electronic Structure, Radiative Transition Probabilities and Integrated IR Absorption Coefficients For AlO, FeO, BaO, UO and UO^+," Technical Report ARPA-IVY OWL Meeting, AVCO Corporation, March 1972.

66. Michels, H. H.: "Ab Initio Calculation of the $B^2\Sigma^+ - X^2\Sigma^+$ Oscillator Strengths in AlO," Journal of Chemical Physics, Vol. 56, p. 665, 1972.

67. Michels, H. H.: Diatomic Oxide Vibrational Band Intensities. Final Report UARL Subcontract RL-98440-S, 1971.

68. Michels, H. H.: Theoretical Determination of Electronic Transition Probabilities for Diatomic Molecules. AFWL Report AFWL-TR-72-1. Final Report For Contract F29601-69-C-0048, May 1972.

69. Michels, H. H.: Theoretical Study of Dissociative-Recombination Kinetics. AFWL Report AFWL-TR-73-288, Final Report for Contract F29601-73-C-0021, May 1974.

70. Michels, H. H.: Theoretical Determination of Metal Oxide f-Numbers. AFWL Report AFWL-TR-74-239, Final Report for Contract F29601-71-C-0119, May 1975.

71. Michels, H. H.: Calculation of Electronic Wavefunctions. AFOSR Report R75-921948, Final Report for Contract F44620-74-C-0083, August 1975.

72. Michels, H. H.: Calculation of Energetics of Selected Atmospheric Systems. AFGL Report AFGL-TR-76-0120. Final Report for Contract F19628-73-C-0300, May 1976.

73. Michels, H. H.: Air Molecular Computation Study. AFGL Report AFGL-TR-77-0032. Final Report for Contract F19628-76-C-0265, March 1977.

74. Michels, H. H.: Calculation of Potential Energy Curves for Metal Oxides and Halides. AFOSR Report R77-921723. Final Report for Contract F44620-73-C-0077, May 1977.

75. Michels, H. H.: "Electronic Structure of Excited States of Selected Atmospheric Systems," The Excited State in Chemical Physics, J. Wm. McGowan, Editor, John Wiley & Sons, Inc., New York, 1981.

76. Hirschfelder, J. O., C. F. Curtiss and R. B. Bird: Molecular Theory of Gases and Liquids, John Wiley & Sons, Inc., New York, 1954.

77. Hirschfelder, J. O. (Ed.): "Intermolecular Forces", Advances in Chemical Physics, Vol. 12, Interscience, New York, 1967.

78. Hopper, D. G.: "MCSCF Potential Energy Surface for the High Barrier Adiabatic $^4\Sigma^-$ Pathway of the $O^+(^4S) + N_2(X^1\Sigma_g^+) \rightarrow NO^+ (X^1\Sigma^+) + N\ (^4S)$ Reaction", Journal of Chemical Physics, 72, p. 3679, 1979.

79. Pipano, A., and J. J. Kaufman: "Ionization Potentials of the N_2O Molecule", Chemical Physics Letters, 7, p. 99, 1970.

80. Pipano, A., and J. J. Kaufmann: "Ab Initio Calculation of Potential Energy Curves for the Ion Molecule Reaction $O^+ + N_2 \rightarrow NO^+ + N$," Journal of Chemical Physics, 56, p. 5258, 1972.

81. Hopper, D. G.: "Ab Initio Study of the N_2O^+ Angular Dependence of the $1^4A''$ ($^4\Pi$) Potential," Chemical Physics Letters, 31, p. 446, 1975.

82. Hopper, D. G.: "Mechanisms of the Reaction of Positive Atomic Oxygen Ions with Nitrogen," Journal of the Americal Chemical Society, 100, p. 1019, 1978.

83. Michels, H. H.: Theoretical Research Investigation Upon Reaction Rates Relating to the Nitric Oxide (Positive) Ion. UTRC Progress Report R79-922102-9, November 15, 1979, United Technologies Research Center, Air Force Geophysics Laboratory Contract AF 19628-77-C-0248.

84. Michels, H. H. and F. E. Harris: "Configuration Interaction Study of the Linear H_3 System," Journal of Chemical Physics, Vol. 48, p. 2371, 1968.

85. Schaefer, J., and W. A. Lester, Jr.: "Theoretical Study of Inelastic Scattering of H_2 by Li^+ on SCF and CI Potential Energy Surfaces," Journal of Chemical Physics, 62, p. 1913, 1975.

86. Michels, H. H. and J. F. Paulson: "Potential Energy Surface and Cross Sections for the $H^-(D^-) + H_2$ (D_2, HD) Ion-Molecule Reaction", Potential Energy Surfaces and Dynamics Calculation, Edited by D. G. Truhlar, Plenum, New York, 1981.

87. Sato, S.: "On a New Method of Drawing the Potential Energy Surface," Journal of Chemical Physics, 23, p. 592, 1955; "Potential Energy Surface of the System of Three Atoms," Journal of Chemical Physics, 23, p. 2465, 1955.

88. For a recent review of semi-empirical potential energy surface functions, see: P. J. Kuntz, "Potential Energy Surfaces and Collisions," Dynamics of Molecular Collisions, Part B, edited by W. H. Miller, Plenum Press, New York, 1976.

89. Morse, P. M.: "Diatomic Molecules According to the Wave Mechanics. II. Vibrational Levels," Physical Review, 34, p. 57, 1929.

90. Hulbert, H. M. and J. O. Hirschfelder: "Potential Energy Functions for Diatomic Molecules," Journal of Chemical Physics, 9, p. 61, 1941.

91. Giese, C. F.: "The Reaction $O^+ + N_2 \rightarrow NO^+ + N$", Advances in Chemistry Series (Ion-Molecule Reaction in Gas Phase), 58, p. 20, 1966.

92. Dunkin, D. B., F. C. Fehsenfeld, A. L. Schmeltekopf, and E. E. Ferguson: "Ion-Molecule Reaction Studies from 300° to 600°K in a Temperature-Controlled Flowing Afterglow System," Journal of Chemical Physics, 49, p. 1365, 1968.

93. Ferguson, E. E., D. K. Bohme, F. C. Fehsenfeld and D. B. Dunkin: "Temperature Dependence of Slow Ion-Atom Interchange Reactions", Journal of Chemical Physics, 50, p. 5039, 1969.

94. Johnsen, R., and M. A. Biondi: "Measurements of the $O^+ + N_2$ and $O^+ + O_2$ Reaction Rates from 300°K to 2 eV," Journal of Chemical Physics, 59, p. 3504, 1973.

95. Kaneko, Y., and N. Kobayashi: "Low-Energy Ion-Neutral Reactions. IV. Formation of NO^+ and N_2^+ in $O^+ + N_2$ Collisions," Journal of the Physical Society of Japan, 36, p. 1649, 1974.

96. Langevin, P.: Analytica Chimica Acta, 5, p. 245, 1905.

97. Gioumousis, G. and D. P. Stevenson: "Reactions of Gaseous Molecule Ions with Gaseous Molecules. V. Theory," Journal of Chemical Physics, 29, p. 294, 1958.

98. Fehsenfeld, F. C., A. L. Schmeltekopf and E. E. Ferguson: "Some Measured Rates for Oxygen and Nitrogen Ion-Molecule Reactions of Atmospheric Importance, Including $O^+ + N_2 \rightarrow NO^+ + N$," Planetary Space Science, 13, p. 219, 1965.

99. McFarland, M., D. L. Albritton, F. C. Fehsenfeld, E. E. Ferguson and A. L. Schmeltekopf: "Flow-drift Technique for Ion Mobility and Ion-Molecule Reaction Rate Constant Measurements. II. Positive Ion Reactions of N^+, O^+ and N_2^+ with O_2 and O^+ with N_2 From Thermal to $\sim$ 2 eV," Journal of Chemical Physics, 59, p. 6620, 1973.

100. Schmeltekopf, A. L., E. E. Ferguson and F. C. Fehsenfeld: "Afterglow Studies of the Reactions He^+, He (2^3S), and O^+ with Vibrationally Excited N_2," Journal of Chemical Physics, 48, p. 2966, 1968.

101. O'Malley, T. F.: "Simple Model for the High Energy Reaction of O^+ Ions with N_2," Journal of Chemical Physics, 52, p. 3269, 1970.

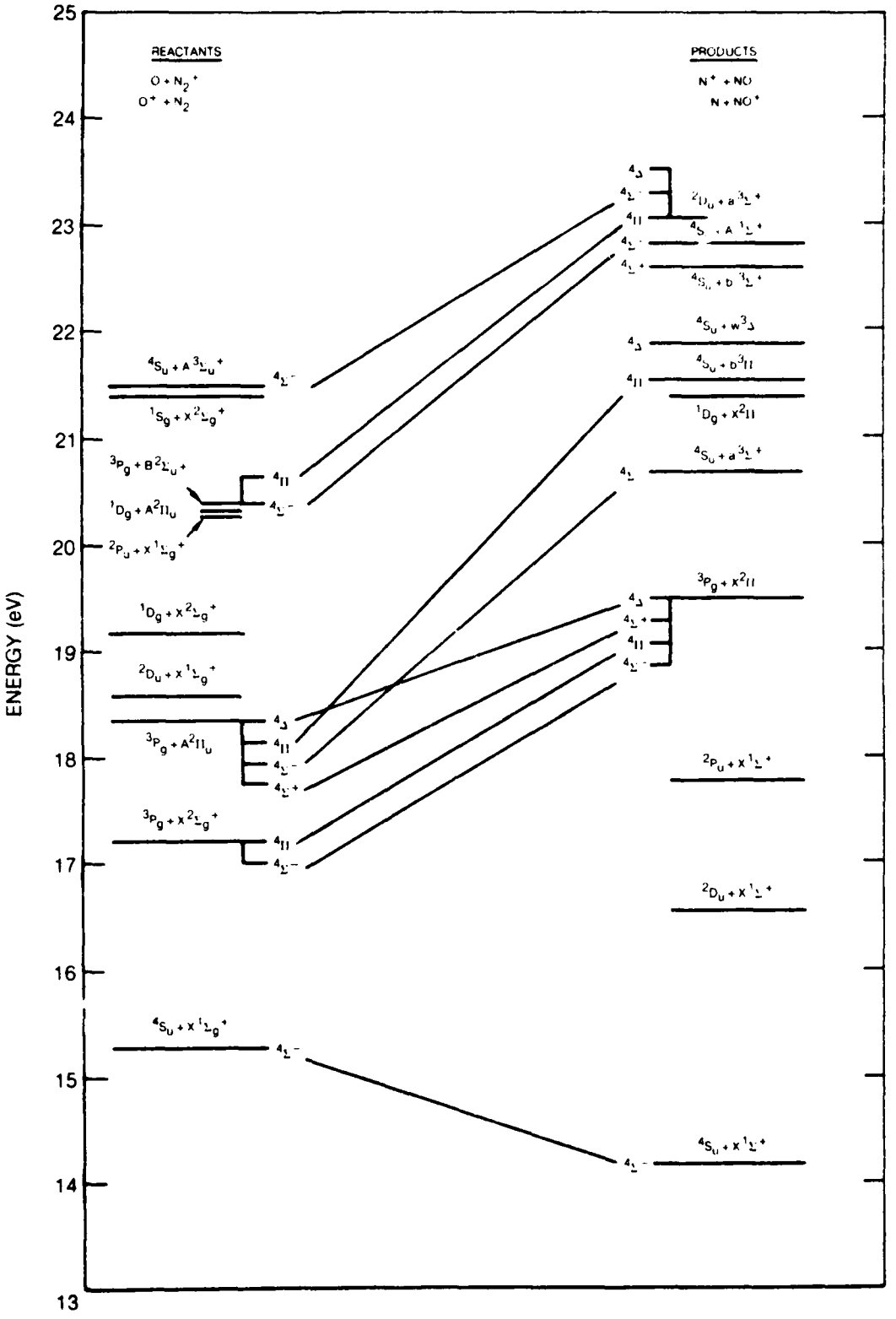

Fig. 1. Molecular Correlation Diagram for the Quartet States of N_2O^+ in $C_{\infty v}$ Symmetry

81-4-36-1

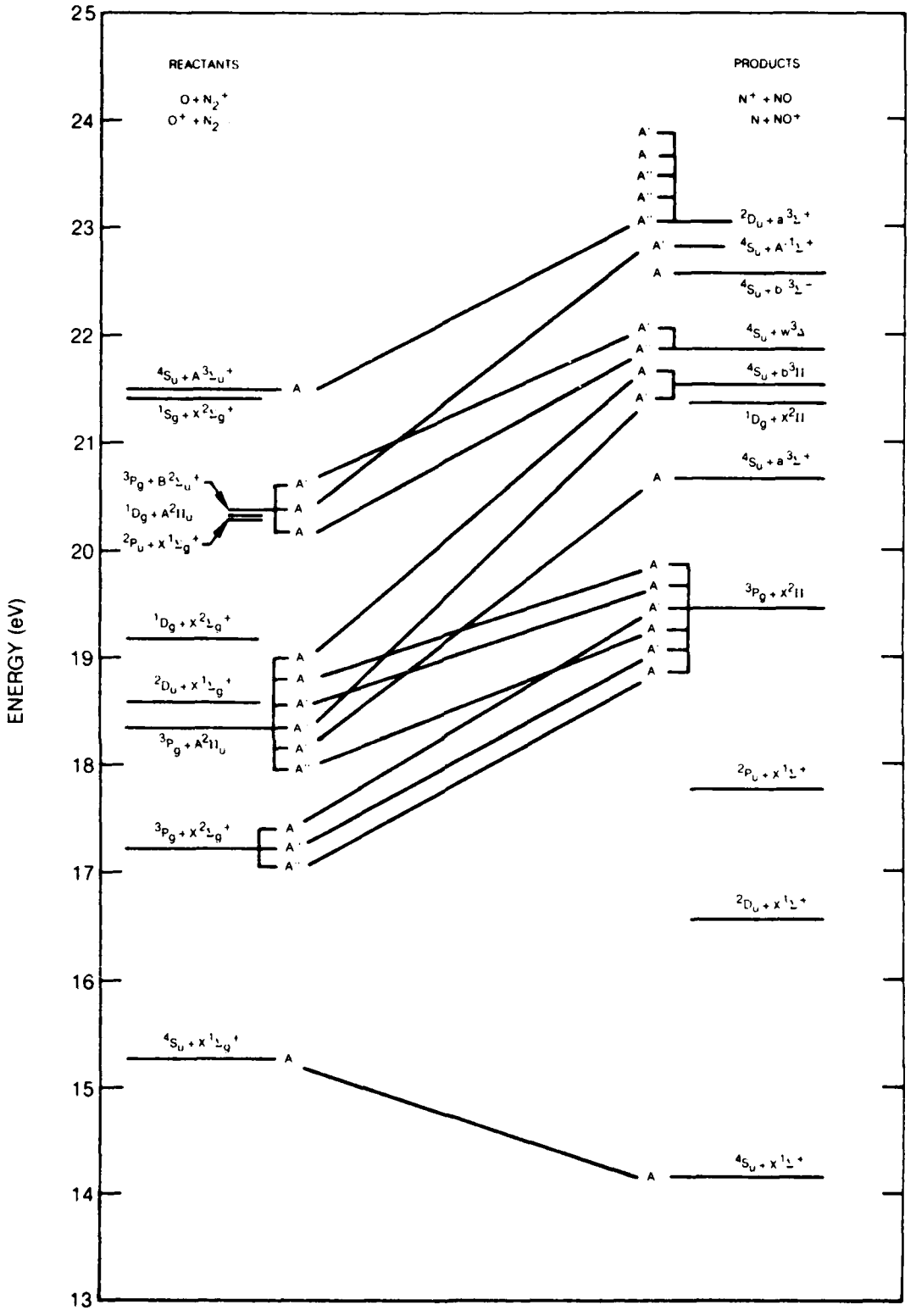

Fig. 2. Molecular Correlation Diagram for the Quartet States of N_2O^+ in C_s Symmetry

81-4-72-3

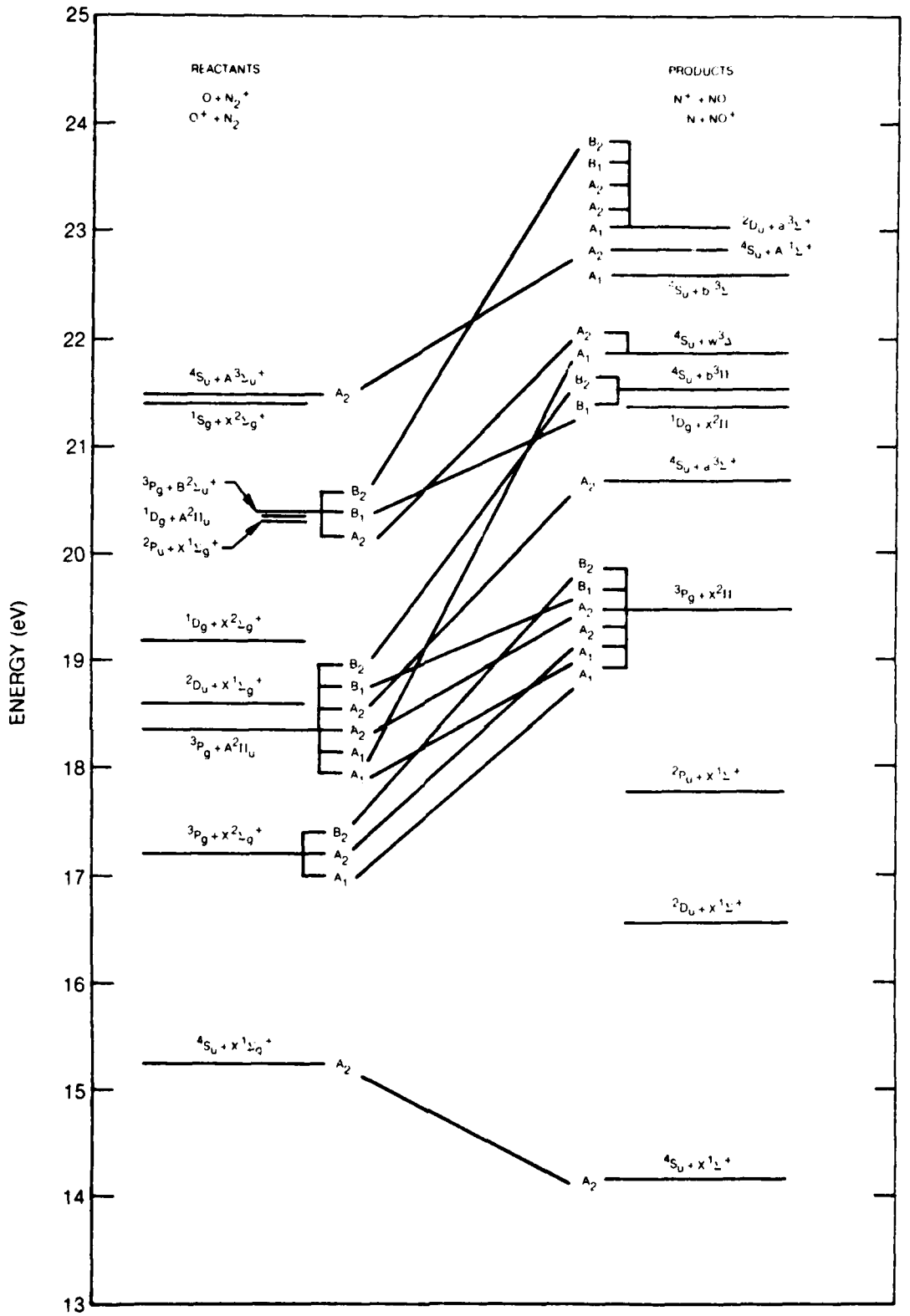

Fig. 3. Molecular Correlation Diagram for the Quartet States of N_2O^+ in C_{2v} Symmetry

81-4-72-4

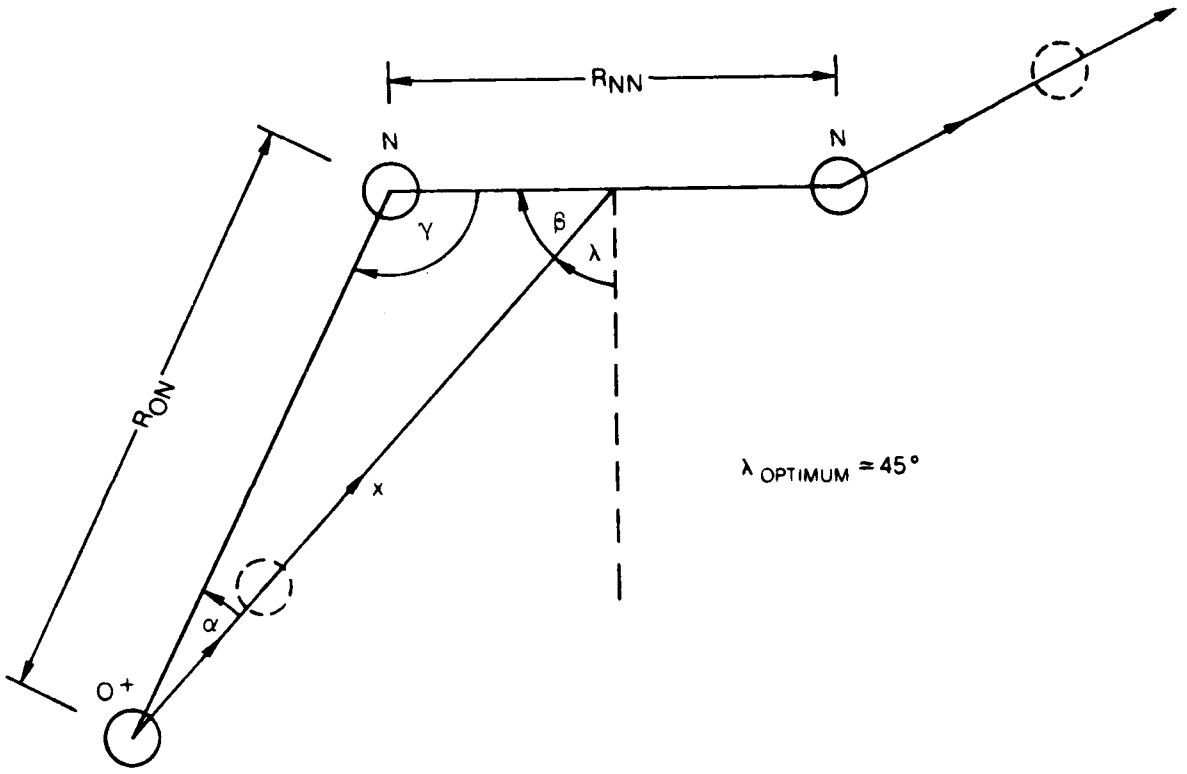

Fig. 4 Reaction Path for $O^+ + N_2 \rightarrow NO^+ + N$

81-4 72-1

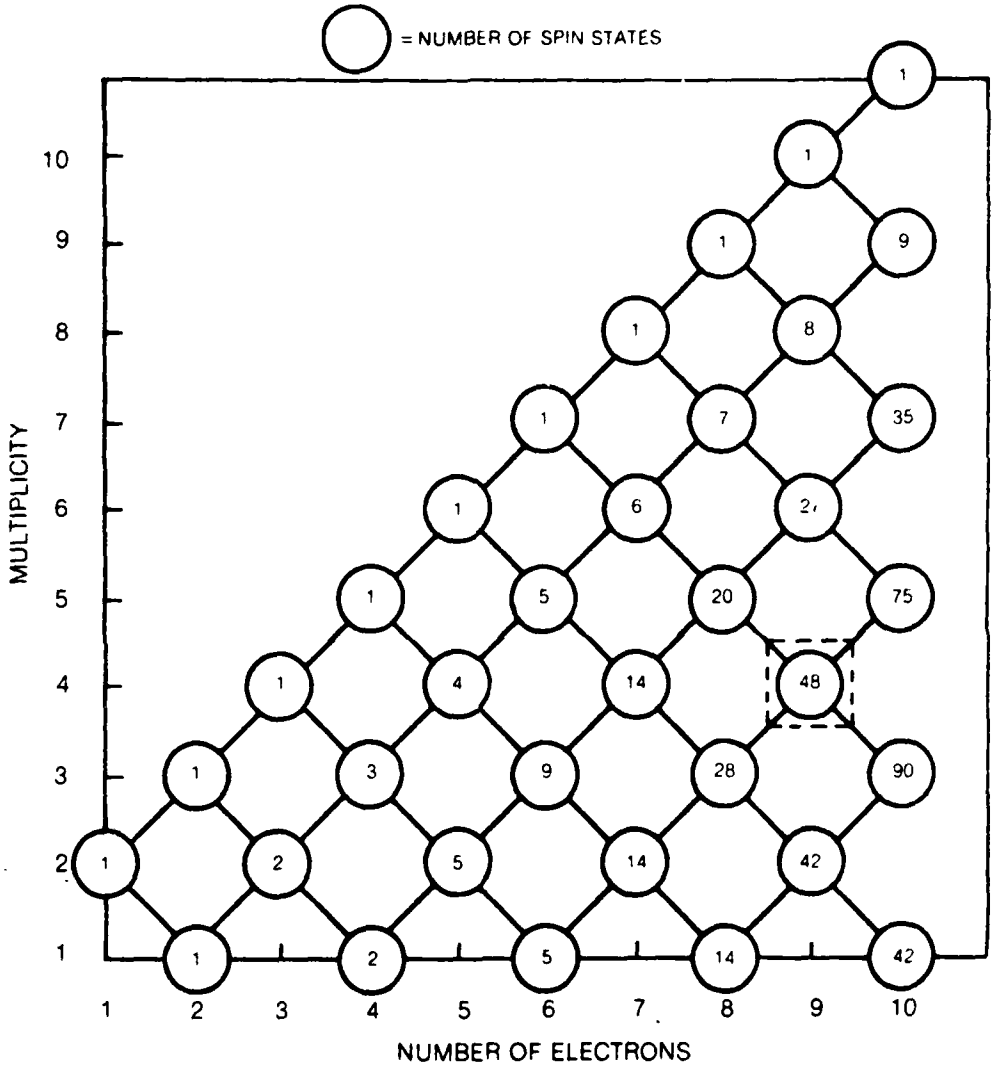

Fig. 5. Vector Coupling Diagram for Electron Spin

80-3-7-4

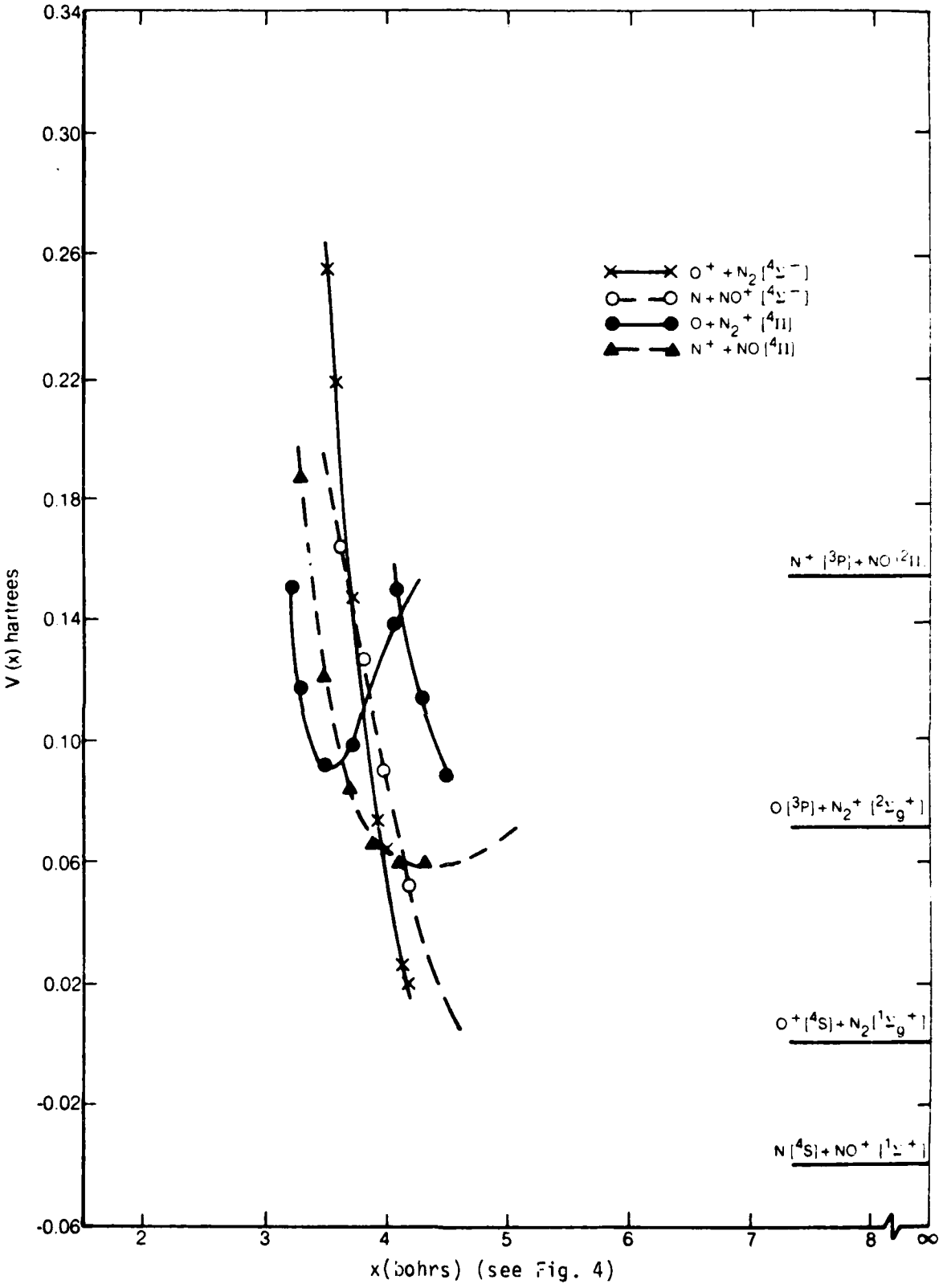

Fig. 6. Potential Surfaces for N_2O^+ in Vicinity of Saddle Region

81-4-116 12

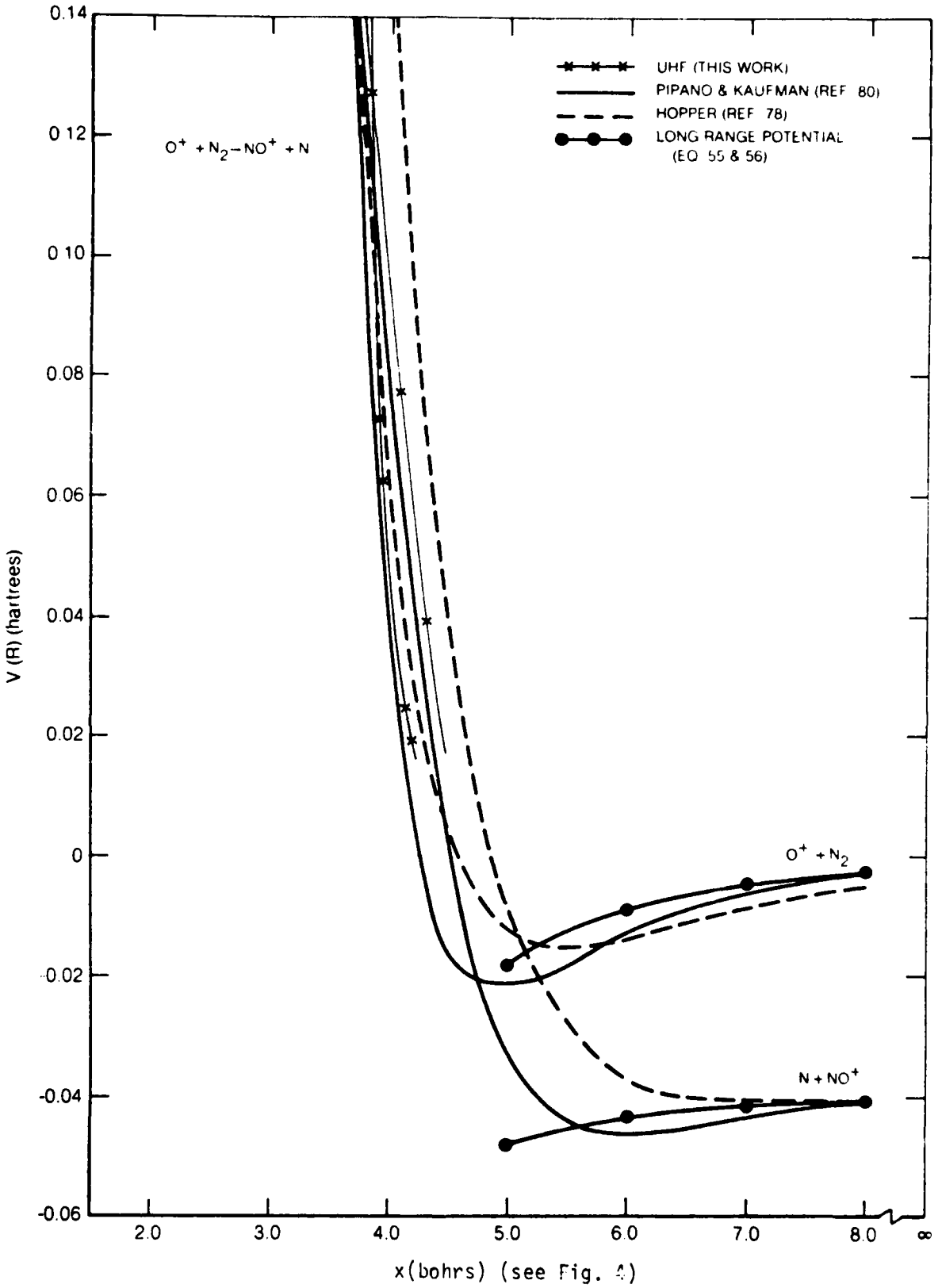

Fig. 7. Linear Reaction Path for $O^+ + N_2 - NO^+ + N$

81-4-116-8

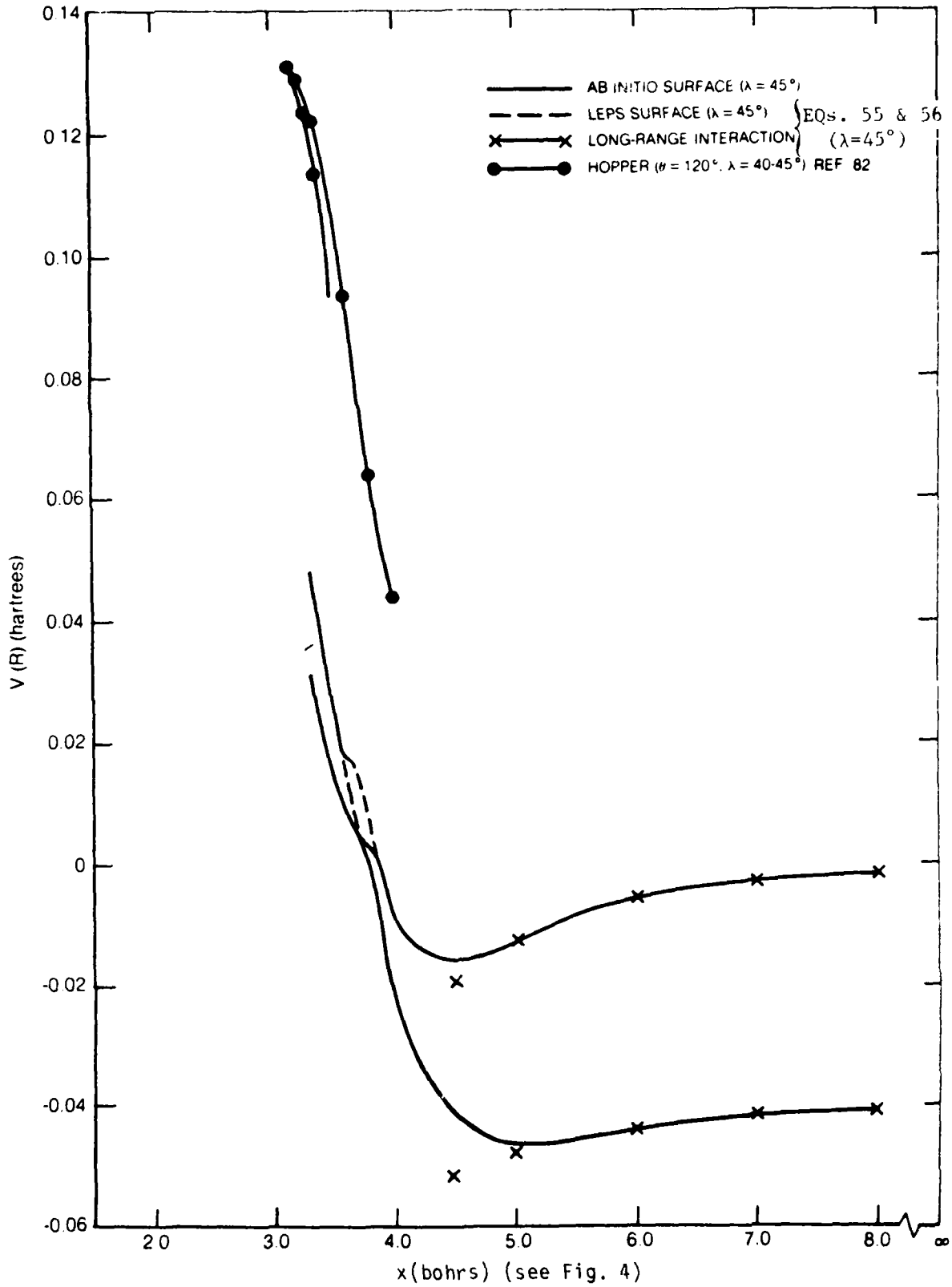

Fig. 8. Reaction Path for $O^+ + N_2 \rightarrow NO^+ + N$ in C_s Symmetry

81-4-116-11

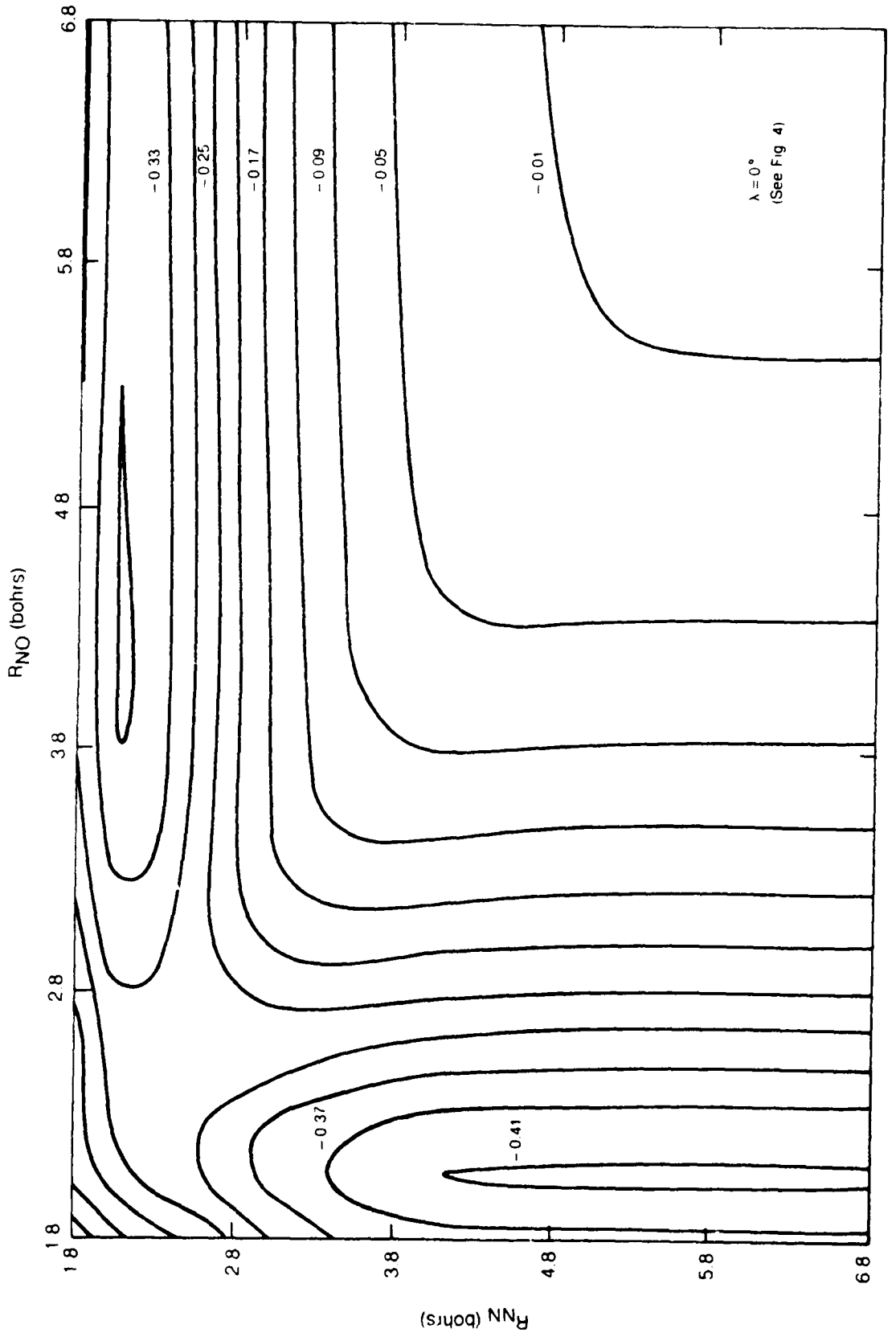

Fig. 9. Contour Plot for N_2O^+ in C_{2v} Symmetry

81-4-116-2

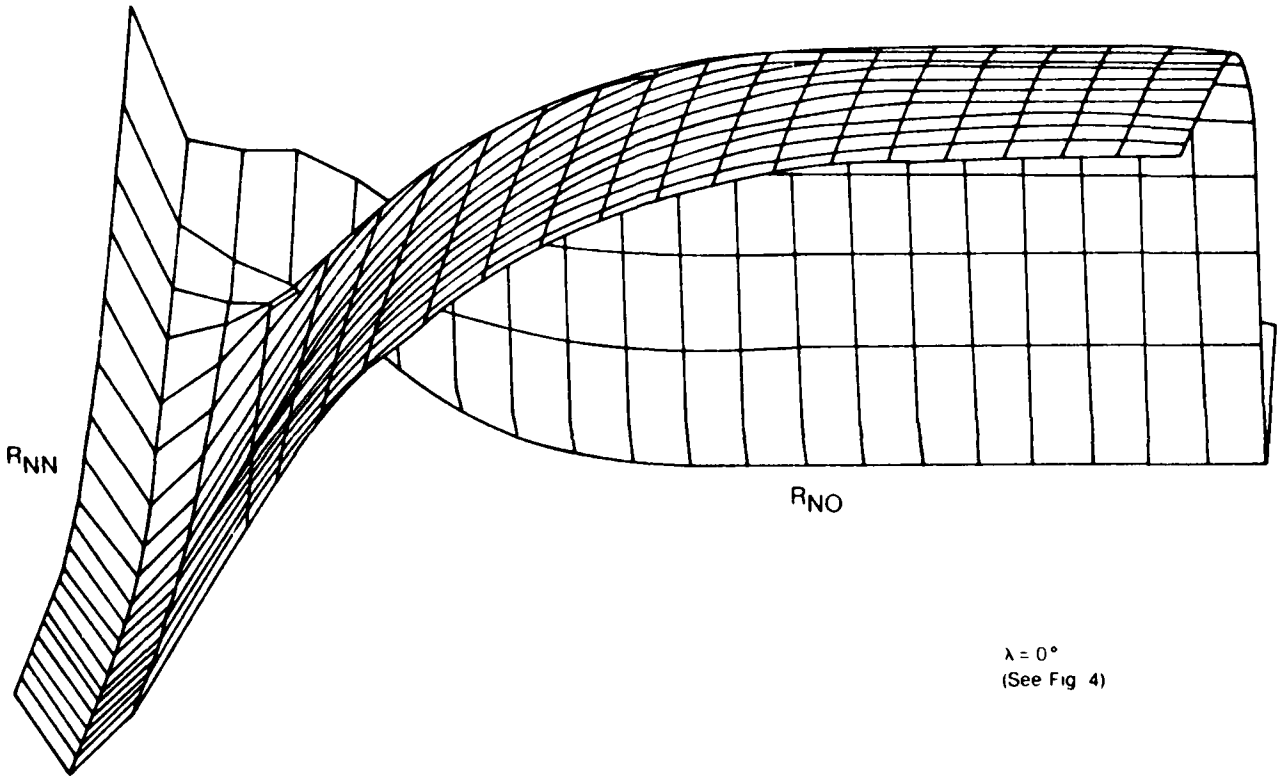

Fig. 10. Reaction Surface for N_2O^+ in C_{2v} Symmetry

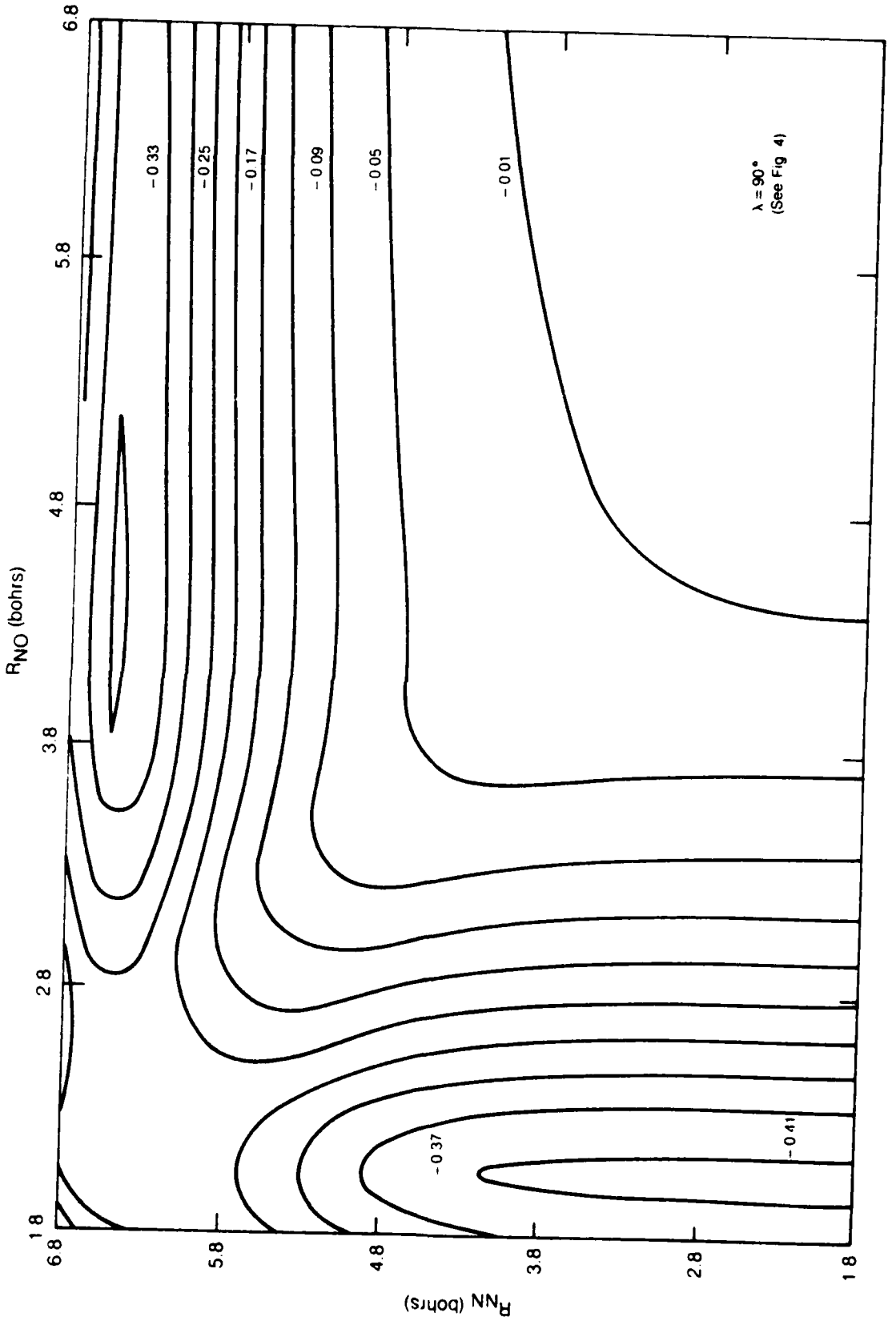

Fig. 11 Contour Plot for N_2O^+ in $C_{\infty v}$ Symmetry

81-4-116-5

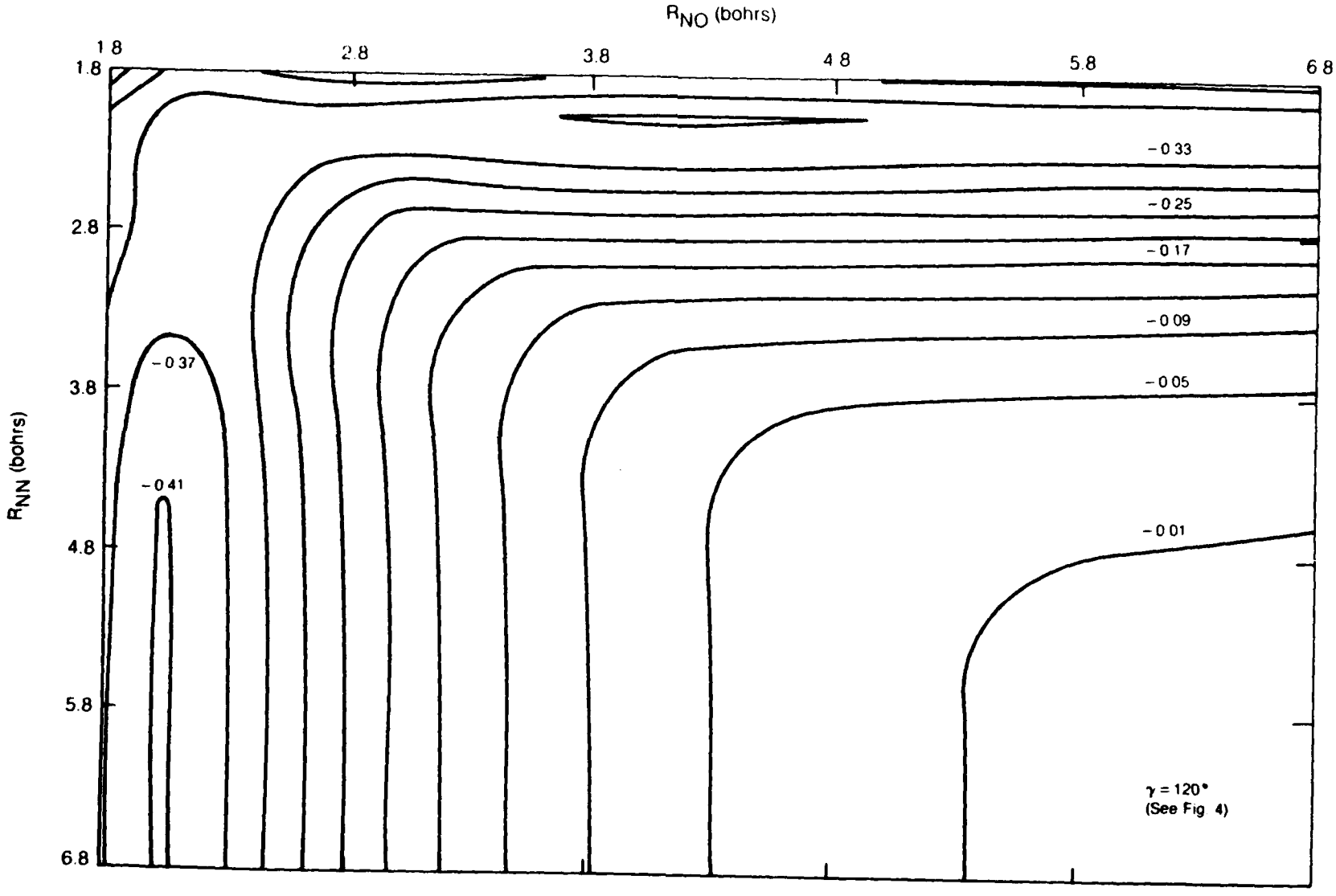

Fig. 12. Contour Plot for N_2O^+ in C_s Symmetry

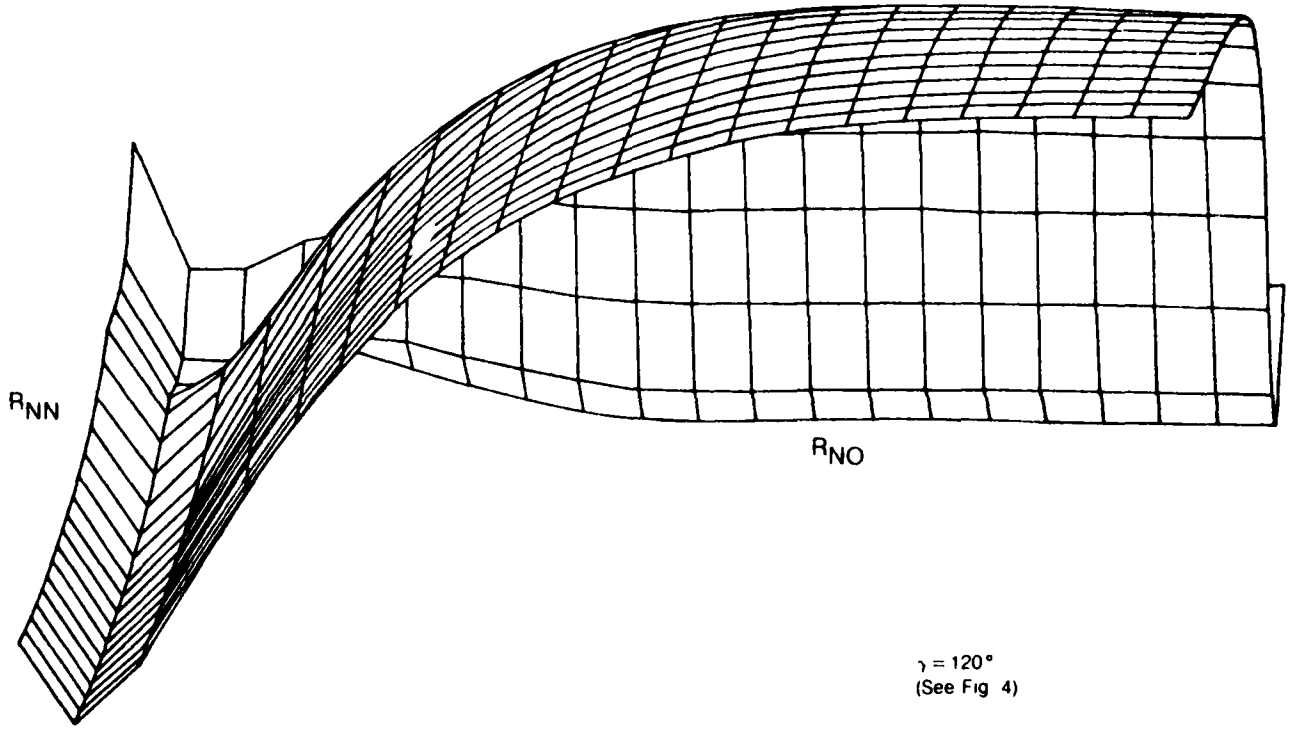

Fig. 13 Reaction Surface for N_2O^+ in C_s Symmetry

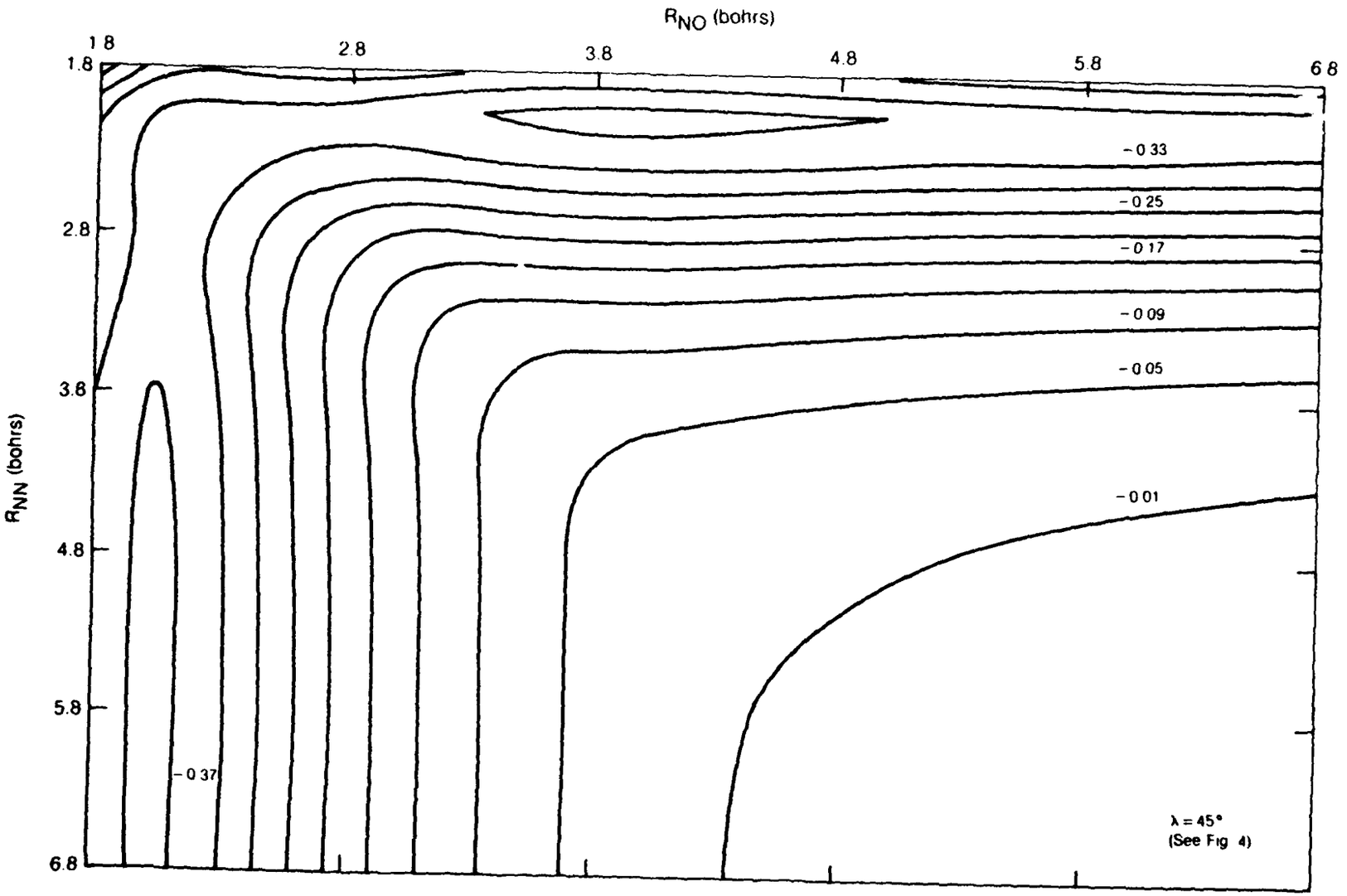

Fig. 14. Contour Plot for Minimum Energy Reaction Surface for N_2O^+

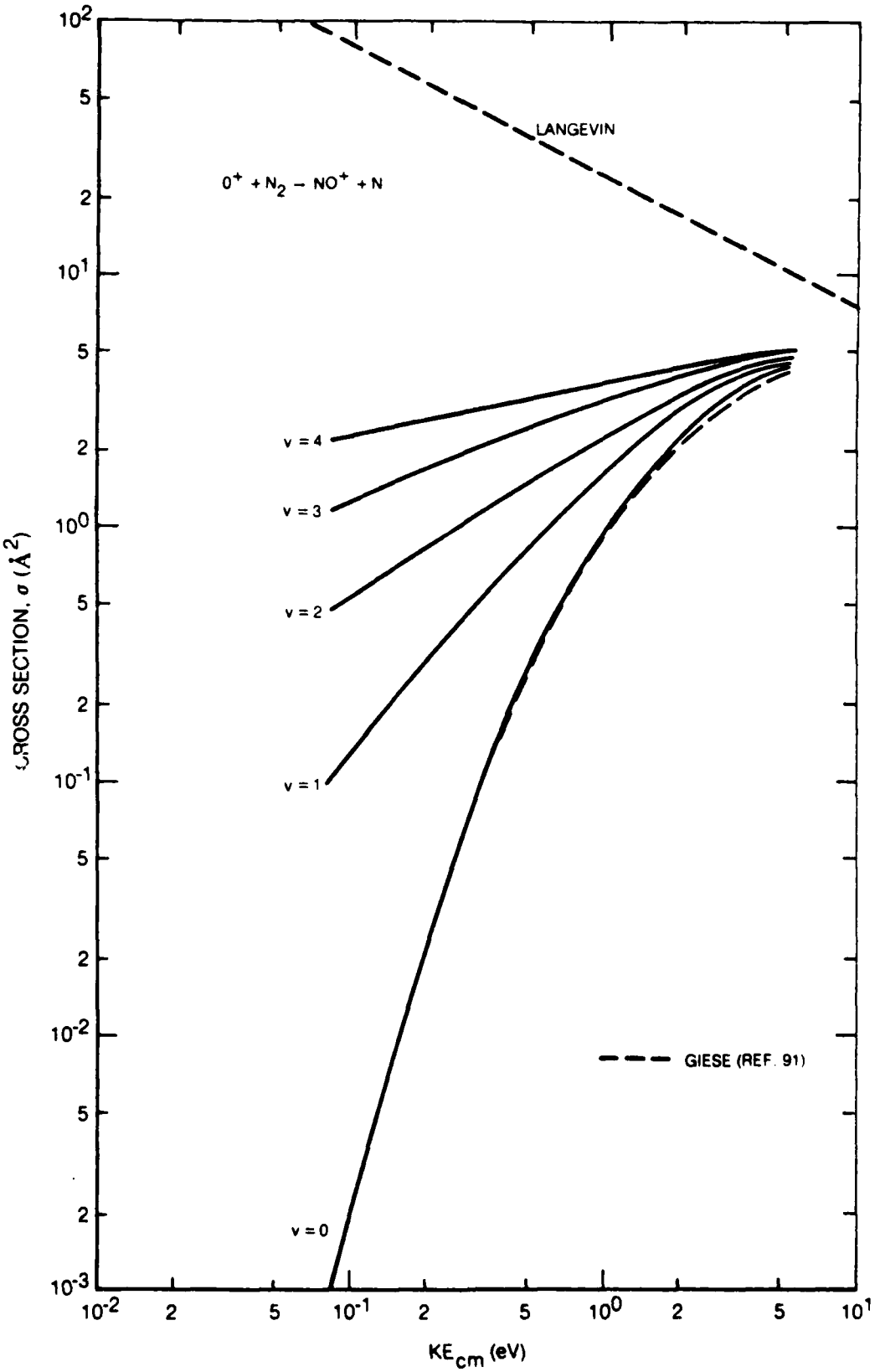

Fig. 15. Reaction Cross Section as a Function of Collision Energy

81-4-116-9

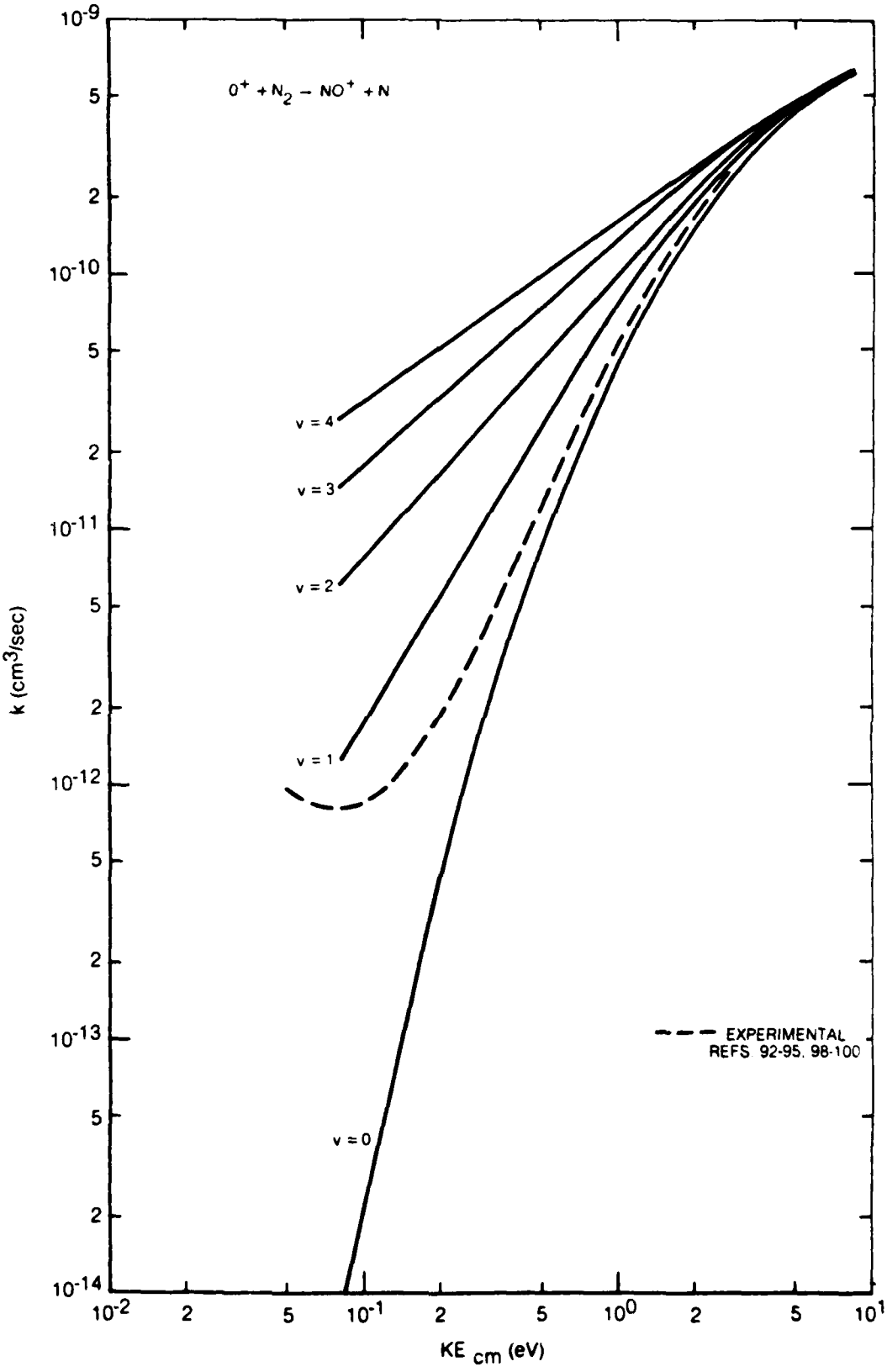

Fig. 16. Reaction Rate Constant as a Function of Collisional Energy

81-4-116-7

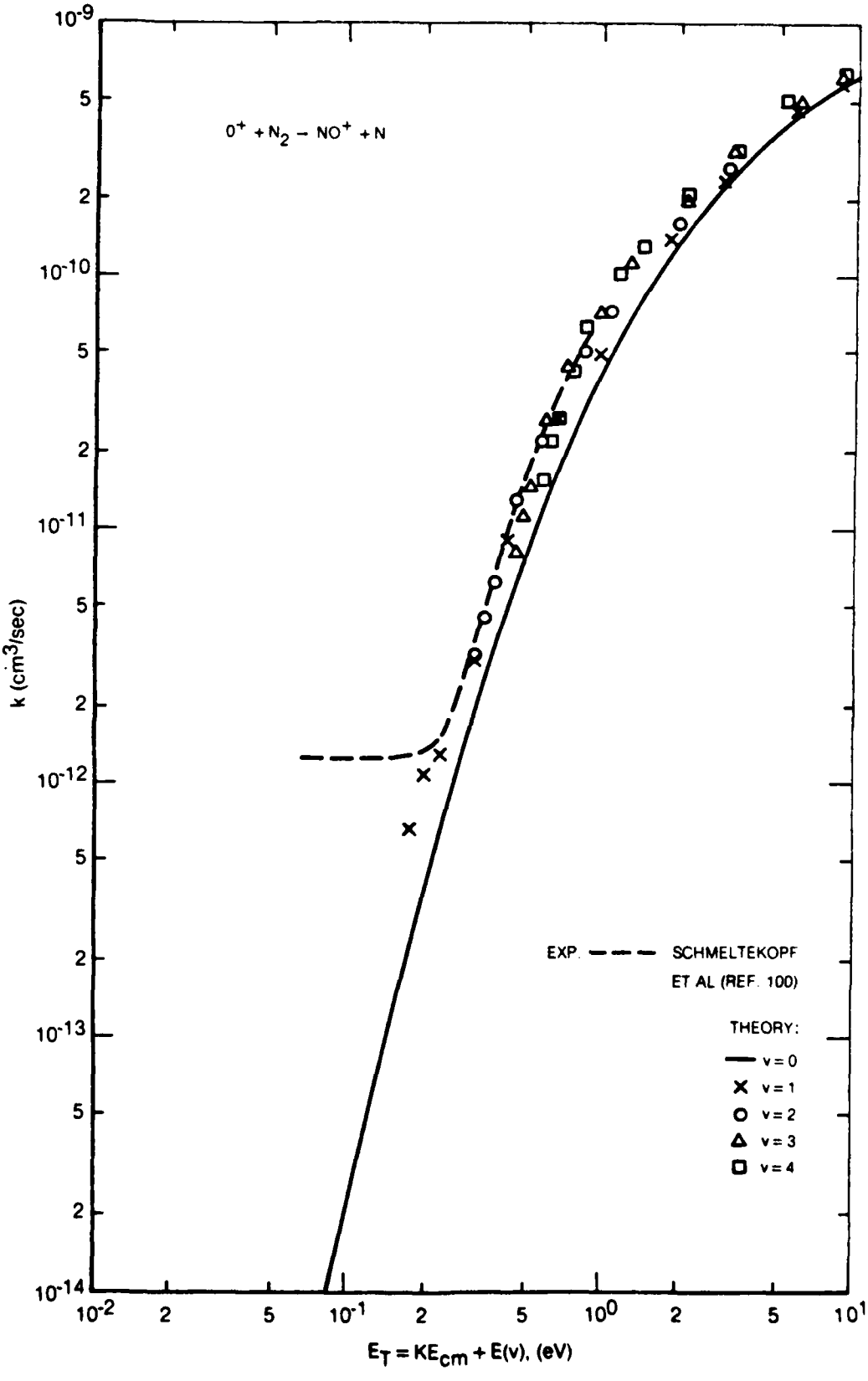

Fig. 17. Reaction Rate Constant as a Function of Total Energy

81-4-116-10

Table 1

MOLECULAR CORRELATION DIAGRAM FOR N_2O^+ (REACTANTS)

Reactants

Dissociation Limit	E(eV)	Electronic States ($C_{\infty v}$)
$N_2\ (X^1\Sigma_g^+) + O^+(^4S_u)$	15.27	$^4\Sigma^-$
$N_2^+(X^2\Sigma_g^+) + O(^3P_g)$	17.21	$^2\Sigma^-$, $^2\Pi$, $^4\Sigma^-$, $^4\Pi$
$N_2^+(A^2\Pi_u) + O(^3P_g)$	18.35	$^2\Sigma^+$, $^2\Sigma^-$, $^2\Pi$, $^2\Delta$, $^4\Sigma^+$, $^4\Sigma^-$, $^4\Pi$, $^4\Delta$
$N_2\ (X^1\Sigma_g^+) + O^+(^2D_u)$	18.59	$^2\Sigma^-$, $^2\Pi$, $^2\Delta$
$N_2^+(X^2\Sigma_g^+) + O(^1D_g)$	19.18	$^2\Sigma^+$, $^2\Pi$, $^2\Delta$
$N_2\ (X^1\Sigma_g^+) + O^+(^2P_u)$	20.29	$^2\Sigma^+$, $^2\Pi$
$N_2^+(A^2\Pi_u) + O(^1D_g)$	20.32	$^2\Sigma^+$, $^2\Sigma^-$, $^2\Pi(2)$, $^2\Delta$, $^2\Phi$
$N_2^+(B^2\Sigma_u^+) + O(^3P_g)$	20.37	$^2\Sigma^-$, $^2\Pi$, $^4\Sigma^-$, $^4\Pi$
$N_2^+(X^2\Sigma_g^+) + O(^1S_g)$	21.40	$^2\Sigma^+$
$N_2(A^3\Sigma_u^+) + O^+(^4S_u)$	21.49	$^2\Sigma^-$, $^4\Sigma^-$, $^6\Sigma^-$

Table 2

MOLECULAR CORRELATION DIAGRAM FOR N_2O^+ (PRODUCTS)

	Products	
Dissociation Limit	E(eV)	Electronic States ($C_{\infty v}$)
$NO^+(X^1\Sigma^+) + N(^4S_u)$	14.18	$^4\Sigma^-$
$NO^+(X^1\Sigma^+) + N(^2D_u)$	16.56	$^2\Sigma^-$, $^2\Pi$, $^2\Delta$
$NO^+(X^1\Sigma^+) + N(^2P_u)$	17.76	$^2\Sigma^+$, $^2\Pi$
$NO(X^2\Pi) + N^+(^3P_g)$	19.45	$^2\Sigma^+$, $^2\Sigma^-$, $^2\Pi$, $^2\Delta$, $^4\Sigma^+$, $^4\Sigma^-$, $^4\Pi$, $^4\Delta$
$NO^+(a^3\Sigma^+) + N(^4S_u)$	20.65	$^2\Sigma^-$, $^4\Sigma^-$, $^6\Sigma^-$
$NO(X^2\Pi) + N^+(^1D_g)$	21.35	$^2\Sigma^+$, $^2\Sigma^-$, $^2\Pi(2)$, $^2\Pi$, $^2\Phi$
$NO^+(b^3\Pi) + N(^4S_u)$	21.52	$^2\Pi$, $^4\Pi$, $^6\Pi$
$NO^+(w^3\Delta) + N(^4S_u)$	21.85	$^2\Delta$, $^4\Delta$, $^6\Delta$
$NO^+(b'^3\Sigma^-) + N(^4S_u)$	22.57	$^2\Sigma^+$, $^4\Sigma^+$, $^6\Sigma^+$
$NO^+(A'^1\Sigma^+) + N(^4S_u)$	22.80	$^4\Sigma^-$
$NO^+(a^3\Sigma^+) + N(^2D_u)$	23.03	$^2\Sigma^-$, $^2\Pi$, $^2\Delta$, $^4\Sigma^-$, $^4\Pi$, $^4\Delta$
$NO^+(W^1\Delta) + N(^4S_u)$	23.04	$^4\Delta$
$NO^+(A^1\Pi) + N(^4S_u)$	23.29	$^4\Pi$
$NO^+(b^3\Pi) + N(^2D_u)$	23.90	$^2\Sigma^+$, $^2\Sigma^-$, $^2\Pi(2)$, $^2\Delta$, $^2\Phi$, $^4\Sigma^+$, $^4\Sigma^-$, $^4\Pi(2)$, $^4\Delta$, $^4\Phi$

Table 3

Long-Range Force Interaction Parameters

	$O^+[^4S]$	$N[^4S]$	$N_2[X^1\Sigma_g^+]$	$NO^+[X^1\Sigma^+]$
$\alpha_{\parallel}$ (bohr^3)	(2.29)	7.42[a,b,c]	16.06	(6.82)[d]
$\alpha_{\perp}$ (bohr^3)	(2.29)	7.42	9.78	(4.12)
Q (bohr^2)	0	0	-0.94[e]	-1.07
I (eV)	35.116[f,g]	14.534	15.581	30.30

[a] R. R. Teachout and R. T. Pack, At. Data 3, 195 (1971).

[b] A. Dalgarno, Adv. Phys. 11, 281 (1962).

[c] J. O. Hirschfelder, et. al., Mol. Theory of Gases and Liquids, Wiley, N.Y. (1954).

[d] The ion polarizabilities are scaled from the corresponding neutral values using the hydrogenic form, $\alpha \sim \sum_i \langle r_i^2 \rangle^2$.

[e] M. Krauss, Natl. Bur. Stand. Tech. Note 438, (1967).

[f] R. L. Kelly and D. E. Harrison, Jr., At. Data 3, 177 (1971).

[g] C. E. Moore, Natl. Bur. Stand. (U.S.) Circ. 467, (1958).

Table 4

Long-Range Interaction Potentials, $O^+ + N_2$ (hartrees)

	V (x, β, R_{NN} = 2.0742 bohrs)		
x (bohrs)	β=0°	β=45°	β=90°
20.0	-.109(-3)	-.553(-4)	-.151(-5)
15.0	-.299(-3)	-.164(-3)	-.284(-4)
10.0	-.129(-2)	-.781(-3)	-.268(-3)
8.0	-.296(-2)	-.187(-2)	-.788(-3)
7.5	-.377(-2)	-.242(-2)	-.107(-2)
7.0	-.490(-2)	-.318(-2)	-.147(-2)
6.5	-.650(-2)	-.428(-2)	-.206(-2)
6.0	-.884(-2)	-.591(-2)	-.298(-2)
5.5	-.124(-1)	-.842(-2)	-.442(-2)
5.0	-.180(-1)	-.124(-1)	-.681(-2)
4.5	-.274(-1)	-.192(-1)	-.110(-1)
4.0	-.440(-1)	-.314(-1)	-.187(-1)
5.4868 (β=0°)	-.1250(-1)	[-.1508(-1)][a]	
5.4740 (β=8.0975°)	-.1245(-1)	[-.1475(-1)]	
5.3722 (β=24.4103°)	-.1210(-1)	[-.1217(-1)]	

[a] Ref. 78. These bracketed values, which are derived from an MC-SCF calculation, appear to overestimate the polarization well for the linear interaction and exhibit an incorrect angular dependence for the long-range interaction.

Table 5

Long-Range Interaction Potential, $N + NO^+$ (hartrees)

	$V(x, \bar{\beta}, R_{NO^+} = 2.0261$ bohrs)		
x (bohrs)	$\bar{\beta}=0°$	$\bar{\beta}=45°$	$\bar{\beta}=90°$
20.0	-.236(-4)	-.235(-4)	-.235(-4)
15.0	-.757(-4)	-.752(-4)	-.748(-4)
10.0	-.398(-3)	-.393(-3)	-.388(-3)
8.0	-.101(-2)	-.990(-3)	-.969(-3)
7.5	-.133(-2)	-.130(-2)	-.127(-2)
7.0	-.178(-2)	-.173(-2)	-.169(-2)
6.5	-.244(-2)	-.237(-2)	-.230(-2)
6.0	-.345(-2)	-.333(-2)	-.322(-2)
5.5	-.505(-2)	-.485(-2)	-.465(-2)
5.0	-.769(-2)	-.734(-2)	-.700(-2)
4.5	-.123(-1)	-.117(-1)	-.110(-1)
4.0	-.212(-1)	-.199(-1)	-.185(-1)
7.3298 ($\bar{\beta}=0°$)	-.146(-2)	[-.832(-3)][a]	

[a] Ref. 78. The bracketed value reported from an MC-SCF calculation underestimates the polarization effects in the exit channel.

Table 6

Potential Energy Surfaces for N_2O^+
in the Vicinity of the Saddle Region

$O^+ + N_2$

x (bohrs)	V(x) (hartrees)	
	$^4\Sigma^-$	$^4\Pi$
∞	0.	+.0713
4.5	--	+.0899
4.3	--	+.1140
4.2	+.0207	--
4.1	+.0265	+.1394 +.1505
4.0	+.0633	--
3.9	+.0737	+.1198
3.8	+.1281	--
3.7	+.1475	+.0992
3.6	+.2188	--
3.5	--	+.0914
3.3	--	+.1166
3.2	--	+.1502

$N + NO^+$

∞	-.0401	+.1536
4.3	--	+.0586
4.2	+.0530	--
4.1	--	+.0603
4.0	+.0901	--
3.9	--	+.0669
3.8	+.1278	--
3.7	--	+.0852
3.6	+.1623	--
3.5	--	+.1213
3.4	--	--
3.3	--	+.1879

Table 7

$^4A''$ Reaction Path Potential Energy
for $O^+ + N_2 \rightarrow NO^+ + N$

Collision Angle = 45°

$O^+ + N_2$

x (bohrs)	V (x) (hartrees)
∞	0.
4.1	-.0050
3.9	-.0029
3.7	+.0037
3.5	+.0129
3.3	+.0313

$NO^+ + N$

x (bohrs)	V (x) (hartrees)
∞	-.0401
4.1	-.0179
3.9	-.0102
3.7	+.0024
3.5	+.0240
3.3	+.0486

Table 8

Reaction Cross Section For $O^+ + N_2(v) \rightarrow NO^+ + N$

KE_{cm} (eV)	σ ($\AA^2$)				
	v = 0	v = 1	v = 2	v = 3	v = 4
.0816	.00069	.102	.499	1.20	2.27
.163	.00937	.178	.755	1.53	2.53
.272	.0576	.401	1.01	1.97	2.87
.544	.339	.876	1.61	2.28	3.21
.816	.704	1.27	1.92	2.93	3.42
1.63	1.90	2.57	2.92	3.74	4.01
2.72	3.19	3.46	3.90	4.47	4.63
5.44	4.28	4.64	4.88	5.01	5.13
8.16	4.70	4.81	4.94	5.09	5.25

Table 9

Reaction Rate Constants For $O^+ + N_2^{\ddagger}(v) \rightarrow NO^+ + N$

KE_{cm} (eV)	k (cm^3/sec)				
	v = 0	v = 1	v = 2	v = 3	v = 4
.0816	9.09(-15)	1.27(-12)	6.20(-12)	1.49(-11)	2.82(-11)
.163	1.65(-13)	3.13(-12)	1.33(-11)	2.70(-11)	4.28(-11)
.272	1.31(-12)	9.10(-12)	2.30(-11)	4.47(-11)	6.51(-11)
.544	1.09(-11)	2.81(-11)	5.19(-11)	7.31(-11)	1.03(-10)
.816	2.77(-11)	5.00(-11)	7.54(-11)	1.15(-10)	1.34(-10)
1.63	1.06(-10)	1.43(-10)	1.63(-10)	2.08(-10)	2.23(-10)
2.72	2.29(-10)	2.48(-10)	2.80(-10)	3.21(-10)	3.33(-10)
5.44	4.35(-10)	4.71(-10)	4.95(-10)	5.09(-10)	5.21(-10)
8.16	5.84(-10)	5.99(-10)	6.15(-10)	6.33(-10)	6.53(-10)

DNA DISTRIBUTION LIST

Department of Defense

Director
Defense Advanced Research Projects Agency
1400 Wilson Boulevard
Arlington, VA 22209

1 cy ATTN: TIO
1 cy ATTN: STO
1 cy ATTN: NRMO

Defense Technical Information Center
Cameron Station, Alexandria, VA 22314

6 cys ATTN: DD

Director
Defense Communications Agency
8th Street and Courthouse Road
Arlington, VA 22204

3 cys ATTN: MEECN Office

12 cys ATTN: TC

Director
Defense Nuclear Agency
Washington, DC 20305

1 cy ATTN: STTL
1 cy ATTN: DDST
3 cys ATTN: RAAE
1 cy ATTN: RAEV
2 cys ATTN: TITL

Joint Chiefs of Staff
Department of Defense
Washington, D. C. 20301

1 cy ATTN: J-6

DNA DISTRIBUTION LIST

Department of Defense (Cont'd)

Director
National Security Agency
Fort George G. Meade, MD 20755

2 cys ATTN: Technical Library

Under Secretary of Defense (Research and Engineering)
Department of Defense
Washington, D. C. 20301

2 cys ATTN: DDS&SS

Department of Commerce

U. S. Department of Commerce
Office of Telecommunications
Institute for Telecommunication Sciences
National Telecommunications and Information Administration
Boulder, CO 80303

2 cys ATTN. W. F. Utlaut

U.S. Department of Commerce
National Bureau of Standards
Washington, D. C. 20234

1 cy ATTN: M. Krauss

Department of the Army

Commander/Director
Atmospheric Sciences Laboratory
U. S. Army Electronics Command
White Sands Missile Range, NM 88002

2 cys ATTN: DELAS-EO
F. E. Niles
M. Heaps

Director
U. S. Army Ballistic Research Laboratories
Aberdeen Proving Grounds, MD 21005

1 cy ATTN: George E. Keller

Department of the Army (Cont'd)

Commander
U. S. Army Foreign Sciences and Technology Center
220 7th Street, N. E.
Charlottesville, VA 22901

1 cy ATTN: Robert Jones

U.S. Army Research Office
Durham, NC 27705

2 cys ATTN: R. Mace

Department of the Navy

Chief of Naval Operations
Department of the Navy
Washington, D. C. 20350

1 cy ATTN: NOP 985
1 cy ATTN: NOP 094H

Office of Naval Research
Department of the Navy
800 North Quincy Street
Arlington, VA 22217

1 cy ATTN: Code 421, B. R. Junker
1 cy ATTN: Code 465, R. G. Joiner
1 cy ATTN: Code 427, H. Mullaney

Commander
Naval Electronic Systems Command
Department of the Navy
Washington, D. C. 20360

1 cy ATTN: PME-117
1 cy ATTN: PME-117T
1 cy ATTN: PME-117-21
1 cy ATTN: PME-117-21A
1 cy ATTN: PME-117-22

Department of the Navy (Cont'd)

Director
Naval Ocean Systems Center
Electromagnetic Propagation Division
271 Catalina Boulevard
San Diego, CA 92152

1 cy ATTN: Code 2200, W. F. Moler
1 cy ATTN: Code 2200, Ilan Rothmuller
1 cy ATTN: Code 2200, John Bickel

Naval Postgraduate School
Monterey, CA 93940

1 cy ATTN: Code 0142
1 cy ATTN: Code 1424

Director
Naval Research Laboratory
4555 Overlook Avenue, S. W.
Washington, D. C. 20375

1 cy ATTN: Code 7700, Timothy P. Coffey
1 cy ATTN: Code 7709, Wahab Ali
2 cys ATTN: Code 7750, John Davis
1 cy ATTN: Code 2627

Commander
Naval Surface Weapons Center (White Oak)
Silver Spring, MD 20910

1 cy ATTN: Technical Library

Office of Naval Research Branch Office
1030 East Green Street
Pasadena, CA 91106

1 cy

DNA DISTRIBUTION LIST

Department of the Air Force

Commander
Air Force Geophysical Laboratory, AFSC
L. G. Hanscom Air Force Base, MA 01731

1 cy ATTN: LKD, W. Swider
1 cy ATTN: LKB, K. Champion
1 cy ATTN: PHG, F. R. Innes
1 cy ATTN: OPR, R. A. Armstrong
1 cy ATTN: OPR, H. Gardiner
1 cy ATTN: LKO, R. E. Huffman
1 cy ATTN: OPR, A. T. Stair
1 cy ATTN: PHI, J. R. Jasperse

Director
Air Force Technical Applications Center
Patrick Air Force Base, FL 32920

1 cy ATTN: TD
1 cy ATTN: HQ 1035th TCHOG/TFS

Commander *AF Weapons Laboratory*
Kirtland AFB, Albuquerque, NM 87117

1 cy ATTN: H. O. Dogliani
1 cy ATTN: J. I. Generosa
1 cy ATTN: SUL

Department of Defense Contractors

General Electric Company
TEMPO - Center for Advanced Studies
816 State Street
Santa Barbara, CA 93102

1 cy ATTN: T. L. Stephens
1 cy ATTN: Warren S. Knapp
1 cy ATTN: DASIAC

Lockheed Missiles and Space Company
3251 Hanover Street
Palo Alto, CA 94304

1 cy ATTN: J. B. Reagan
1 cy ATTN: W. Imhof
1 cy ATTN: Martin Walt

Department of Defense Contractors (Cont'd)

Mission Research Corporation
735 State Street
Santa Barbara, CA 93101

1 cy ATTN: M. Scheibe
1 cy ATTN: D. Sowle

Pacific-Sierra Research Corporation
1456 Cloverfield Boulevard
Santa Monica, CA 90404

1 cy ATTN: E. C. Field

Pennsylvania State University
Ionospheric Research Laboratory
College of Engineering
318 Electrical Engineering - East Wing
University Park, PA 16802

1 cy ATTN: John S. Nisbet
1 cy ATTN: Les Hale
1 cy ATTN: A. J. Ferraro
1 cy ATTN: H. S. Lee

R&D Associates
4640 Admiralty Way
Marina Del Rey, CA 90291

1 cy ATTN: R. Lelevier
1 cy ATTN: F. Gilmore
1 cy ATTN: R. Turco

The Rand Corporation
1700 Main Street
Santa Monica, CA 90406

1 cy ATTN: Cullen Crain

Professor Chalmers F. Sechrist
155 Electrical Engineering Building
University of Illinois
Urbana, IL 61801

1 cy ATTN: C. Sechrist

Department of Defense Contractors (Cont'd)

SRI International
333 Ravenswood Avenue
Menlo Park, CA 94025

1 cy ATTN: Allen M. Peterson
1 cy ATTN: Ray L. Leadabrand
1 cy ATTN: J. R. Peterson
1 cy ATTN: F. T. Smith

University of Pittsburgh
Dept. of Physics and Astronomy
Pittsburgh, PA 15260

1 cy ATTN: M. A. Biondi
1 cy ATTN: F. Kaufman
1 cy ATTN: W. Fite
1 cy ATTN: J. N. Bardsley
1 cy ATTN: E. Zipf

General Electric Co., Space Division, VFSC
Goddard Blvd., King of Prussia
P. O. Box 8555
Philadelphia, PA 19101

1 cy ATTN: M. H. Bortner

National Oceanic & Atmospheric Admin.
Environmental Research Laboratories
Dept. of Commerce
Boulder, CO 80302

1 cy ATTN: E. E. Ferguson
1 cy ATTN: F. Fehsenfeld

Photometrics, Inc.
442 Marrett Road
Lexington, MA 02173

1 cy ATTN: I. L. Kofsky

Department of Defense Contractors (Cont'd)

Harvard College Observatory
Cambridge, MA 02138

1 cy ATTN: A. Dalgarno
1 cy ATTN: D. E. Freeman

Utah State University
Logan, UT 84322

1 cy ATTN: K. D. Baker

United Technologies Research Center
East Hartford, CT 06108

1 cy ATTN: G. A. Peterson
1 cy ATTN: H. H. Michels

Stewart Radiance Laboratories
1 De Angelo Drive
Bedford, MA 01730

1 cy ATTN: R. D. Sharma
1 cy ATTN: J. C. Ulwick

Aerodyne Research, Inc.
Crosby Drive
Bedford, MA 01730

1 cy ATTN: M. Camac

Visidyne, Inc.
NW Industrial Park
Burlington, MA 01803

1 cy ATTN: T. C. Degges
1 cy ATTN: C. H. Humphrey
1 cy ATTN: H. J. R. Smith

Physical Sciences, Inc.
Lakeside Office Park
Wakefield, MA 01880

1 cy ATTN: G. Caledonia
1 cy ATTN: T. Rawlins

Department of Defense Contractors (Cont'd)

Jet Propulsion Laboratory, CIT
Pasadena, CA 91103

1 cy ATTN: S. Prasad

BC Space Data Analysis Laboratory
885 Centre Street
Newton, MA 02159

1 cy ATTN: S. Guberman

R&D Associates
1401 Wilson Boulevard
Arlington, VA 22209

1 cy ATTN: H. Mitchell

Lockheed Missile and Space Company, Inc.
Huntsville, AL 35803

1 cy ATTN: D. Divis
1 cy ATTN: C. M. Bowden

Spectral Sciences, Inc.
99. S. Bedford Street
Burlington, MA 01803

1 cy ATTN: F. Bien

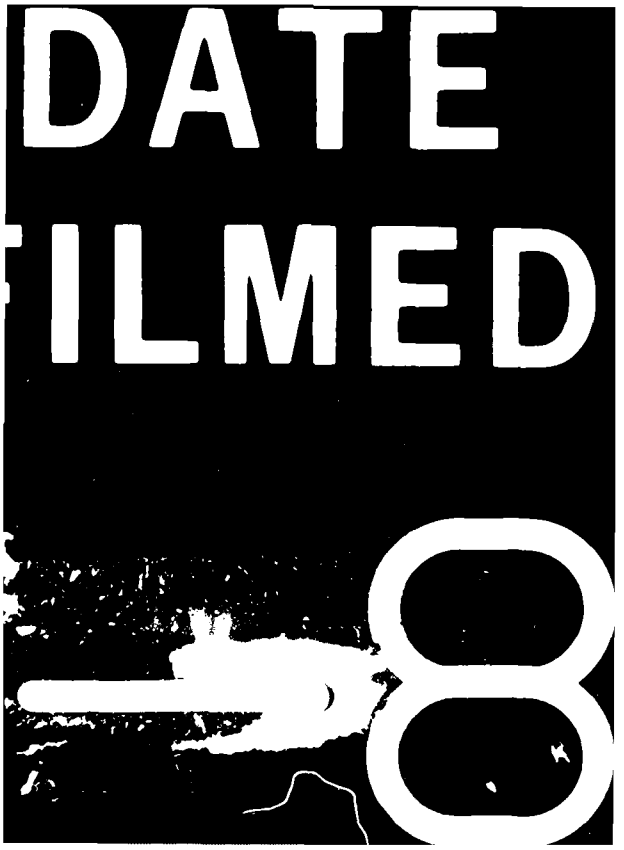
DATE
ILMED
8